MSc Thesis

Laminar burning velocity measurements of DNG with hydrogen addition

V. Margos

Technische Universiteit Delft

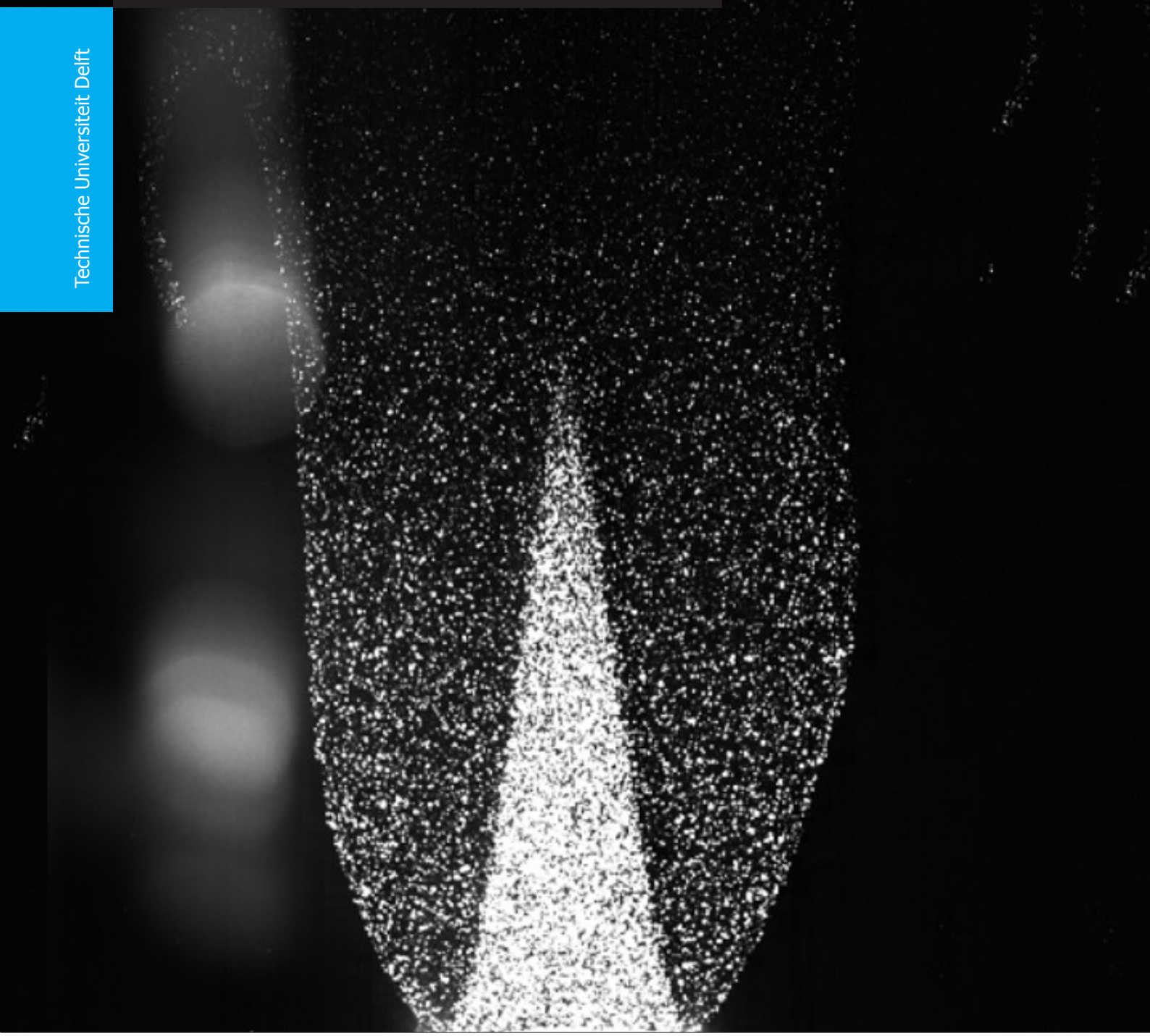

TU Delft Delft University of Technology

Challenge the future

MSc Thesis

Laminar burning velocity measurements of DNG with hydrogen addition

by

V. Margos

in partial fulfillment of the requirements for the degree of

Master of Science
in Aerospace engineering

at the Delft University of Technology,
to be defended publicly on Monday January 21, 2019 at 10:00 AM.

Supervisor:	Dr. ir. A. Bohlin	
	Dr. ir. J. Steimes	
Thesis committee:	Dr. ir. A. Gangoli Rao,	TU Delft
	Dr. ir. M. J. Tummers,	TU Delft

This thesis is confidential and cannot be made public until December 31, 2019.

TU Delft Delft University of Technology

Summary

The worldwide gas emissions regulations are getting more stringent. Together with the fluctuations of the finite fuel resources, it is expected that the use of unconventional and renewable fuels will increase. Hydrogen fuel is a zero-emission, renewable energy source. It has a great potential as one of the principal sustainable energy sources of the future. A gradual conversion to a hydrogen based energy system, if the necessary government framework is provided, is far more likely to happen. This opportunity can be found in the natural gas grid of the Netherlands. This natural gas infrastructure is accessible for both the industry and Dutch households. The IEA HGH RD programme has conducted research about this gradual transition, with promising results. It is currently therefore a key agenda point for the Dutch government. In order to safely make a transition to natural gas with hydrogen addition, it is of importance to know the fundamental combustion properties of these fuel mixtures. These properties are needed for the prediction of and modeling of combustion systems. Traditionally, the quantification of the combustion process is done by focusing on measuring properties such as laminar burning velocity, ignition and extinction characteristics, flammability limits and emissions. The laminar burning velocity is an important property of combustion mixtures. It contains fundamental information on reactivity, exothermicity and diffusivity.

This thesis has investigated the laminar burning velocity of Dutch natural gas - hydrogen mixtures numerically and experimentally. The volumetric addition of hydrogen up to 50% was investigated in 10% increments. Experimental measurements were performed with the Bunsen burner method. Two experimental methodologies were applied to obtain the laminar burning velocity. The mass conservation method was used in combination with the OH*-chemiluminescence. The second methodology used the semi-cone angle method in combination with Particle image velocimetry (PIV). 12 different conditions were measured with PIV. These points are for 3 different fuel compositions (0, 20 and 50% H_2), two different equivalence ratios (1.0 and 1.4) and two different flow conditions (1100/1600 and 1800 Reynolds). The PIV methodology obtained measurements are compared with both OH*-chemiluminescence and the numerical calculations. The effect of the flow conditions on the PIV measured laminar burning velocity was also investigated. Numerical predictions were obtained with the GRI-Mech 3.0 kinetic mechanism. Preliminary measurements were performed with 100% hydrogen in order to validate the optical diagnostics and post-processing procedure for the OH*-chemiluminescence methodology.

The measurements from both independent measurement techniques, PIV and OH*, are in good agreement with each other for all measured equivalence ratios. The DNG/hydrogen measurements with OH*-chemiluminescence can be interpreted with great confidence due to the successful hydrogen validation methodology. Therefore conclusions can be drawn that PIV is a reliable method to obtain the laminar burning velocity without typical uncertainties found with OH*-chemiluminescence, primarily due to the mass flow controllers, since the actual velocity field is obtained. It was found, however, from comparing the velocities obtained for different flow conditions, that the seeding disturbance and thermophoretic effects can have a significant effect on the PIV laminar burning velocity results. These influences should therefore be approached with care when using PIV. OH*-chemiluminescence shows a larger uncertainty interval due to the mass flow controllers. The advantages of this measurement technique however are the ease of use and low cost when compared to PIV. Numerical results obtained with GRI-Mech 3.0 are in good agreement with OH*-chemiluminescence and PIV results for equivalence ratios 1.2 and lower. Large discrepancies in the range 20-35% are observed in the rich region for equivalence 1.3 - 1.5. These discrepancies are consistent with both PIV and OH*-chemiluminescence measurements. These discrepancies could be attributed to the validity of the kinetic mechanism for the composition of DNG, which contains methane with higher order hydrocarbons and 14% N_2, in the rich region. The DNG from the Dutch gas network could also have a different composition than the one used for the numerical simulation resulting in different laminar burning velocities.

Preface

I would like to thank both my supervisors dr. Alexis Bohlin and dr. Johan Steimes. I am grateful for the time they have spent in guiding and tutoring me throughout my thesis project. I would also like to thank Bart Hoek for assisting me in performing the experiments. Lastly I would like to thank the Process and Energy department of the faculty of Mechanical, Maritime and Materials Engineering, for giving me the opportunity to conduct my experiments in their combustion laboratory.

V. Margos
Delft, December 2018

Contents

List of Figures

List of Tables

Nomenclature

Latin symbols

T	Temperature
h	Enthalpy
C_p	Specific heat capacity
d_p	Particle diameter
D	Mass diffusivity
D_H	Hydraulic diameter
f	fuel-to-air ratio
Ka	Karlovitz number
K	Stretch rate
Le	Lewis number
nm	Nanometer
ns	nanosecond
$\dot{Q}$	Volumetric flow rate
Re	Reynolds number
S_L	Burning velocity
$S_{L,u}$	unstretched burning velocity
S_S	Spatial velocity
S_{ug}	Unburned gas velocity
u′	turbulence parameter
A_f	Flame front area
Z	Critical value
n	sample size
Hz	Hertz
Stk	Stokes' number

Greek symbols

α	Power coefficient temperature
β	Power coefficient pressure
ϕ	Equivalence ratio
λ	Thermal conductivity
ρ	Density
δ	flame thickness
$\dot{\omega}$	Reaction rate
ν	Kinematic viscosity
μ	Dynamic viscosity
σ	Standard deviation

List of abbreviations

CCD	Charge-coupled device
DNG	Dutch natural gas
FAR	Fuel-to-air ratio
PIV	Particle image velocimetry
MFC	Mass flow controller

1

Introduction

In this chapter, the research topic is introduced, with the title: 'the laminar burning velocities of Dutch natural gas (DNG) with hydrogen addition'. Firstly, the importance and background of this research is given. Then, the laminar burning velocity is elaborated upon in detail. After that, a brief summary of the different prominent measurement techniques available for the burning velocity is elaborated upon. This is followed by an analysis of the current scientific background. Lastly, the research objective is given, followed by an outline of the report.

1.1. Background

The worldwide gas emissions regulations are getting more stringent. Together with the fluctuations of the finite fuel resources, it is expected that the use of unconventional and renewable fuels will increase. Hydrogen fuel is a zero-emission, renewable energy source. It has a great potential as one of the principal sustainable energy sources of the future. A gradual conversion to a hydrogen based energy system, if the necessary government framework is provided, is far more likely to happen. This opportunity can be found in the natural gas grid of the Netherlands. This natural gas infrastructure is accessible for both the industry and Dutch households. The IEA HGH RD programme has conducted research about this gradual transition, with promising results [9]. It is for this reason currently a key agenda point for the Dutch government [10].

Natural gas is also considered to be a favorable fuel for spark-ignited and compression-ignited engines. These engines however are mostly operating near the stoichiometric equivalence ratio. This is due to the slow burning velocity of natural gas, which causes poor lean-burn ability. These engines have the disadvantage of low thermal efficiency, large cycle-by-cycle variation, and poor performance in the lean region, which results in increased fuel consumption and decreased engine power output [11, 12].

The traditional way to improve the lean-burn capabilities of natural gas engines, is to increase the flow intensity in the cylinders for lean-burning, by increasing the charge turbulence and density [13]. This, however, results in increased heat losses and NOx emissions due to increased combustion temperature. One effective method to increase the burning velocity of natural gas, is with the addition of hydrogen. It is regarded as the best gaseous addition to natural gas for this purpose, due to its very high burning velocity and also decreased CO_2 emissions.

In order to safely make a transition to natural gas with hydrogen addition, it is of importance to know the fundamental combustion properties of these fuel mixtures. These properties are needed for the prediction of and modeling of combustion systems. Traditionally, the quantification of the combustion process is done by focusing on measuring properties such as laminar burning velocity, ignition and extinction characteristics, flammability limits and emissions [14]. The laminar burning velocity is an important property of combustion mixtures. It contains fundamental information on reactivity, exothermicity and diffusivity [15]. It is useful for gas turbine design, as it is used for the understanding

and development of empirical models for flame propagation of homogeneous fuel-air mixtures, ignition energy requirements, and other conditions of interest for gas turbines [16]. Nearly all practical combustion systems create flow conditions that are turbulent, since this increases the mass consumption rate of the reactants to values significantly greater than those obtained with laminar flames. The laminar burning velocity however is of importance for the understanding and development of models regarding the turbulent burning velocity [17].

The current combustion and burner systems are developed for a specific natural gas composition. Natural gas is a mixture of several hydrocarbons and inert gases. The variation is dependent on the geographical location. DNG for example consists of 81.3% methane, volumetrically. Hydrogen addition to Dutch natural gas will likely have consequences for these systems in their operation and design. The combustion properties of Dutch natural gas hydrogen mixtures are therefore of importance. The laminar burning velocity, a key property, will be the focus of this research. In the next section, this parameter is further explained.

1.2. Laminar burning velocity

One of the important properties of combustion processes, the laminar burning velocity, is further elaborated in this section. Firstly, the definition of the laminar burning velocity is introduced. The flame structure is also addressed. Secondly, the parameters which influence and disturb the laminar burning velocity are explained. In the last part the relation to turbulent combustion modelling is addressed.

1.2.1. Definition of the burning velocity

A flame can be defined as a self-sustaining chemical reaction [1]. A premixed flame is obtained when the fuel and oxidizer are completely mixed into a homogeneous mixture prior to combustion. The flame front is associated with a flame, in which the unburned gas mixture is heated and converted into products. This flame front is a thin region of space in which most of the combustion reaction takes place. The flame front can be split up in two regions, called the preheat and reaction zone, as depicted in figure 1.1.

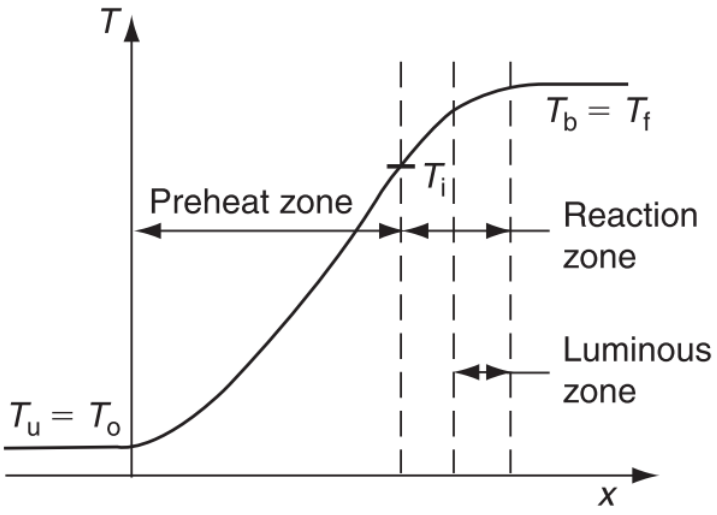

Figure 1.1: Flame front structure [1]

The preheat zone starts at the cold boundary, denoted as T_u in figure 1.1, and ends at the ignition temperature, T_i. The temperature rise of the unburned gas in the preheat zone is mainly due to heat conduction, and some convection from the reaction zone. The temperature rise is concave upwards, because each element in this region acts as a heat sink. The temperature increase results in the expansion and acceleration of the unburned gas. There are no significant chemical reactions happening in this region [18].

The gaseous mixture start undergoing chemical reactions upon reaching the ignition temperature, with a temperature increasing in a concave downwards manner, until it reaches its final equilibrium

temperature, which is denoted as T_f. This region is referred to as the reaction zone. This reaction zone is subdivided into the primary, denoted as the luminous zone, and the secondary zone. The secondary zone is associated with weak secondary luminosity [19]. This whole region, consisting of the preheat and reaction zone, generally has a significant thickness. This is denoted as the flame front thickness.

The laminar burning velocity is defined as the velocity at which the flame propagates into the reactant mixture. This velocity, S_L, as can be seen in figure 1.2 pointing towards the unburned gas mixture, normal to the flame front. The unburned mixture has a velocity denoted by S_{UG}. The flame front will only remain in a fixed position if the laminar burning velocity is equal to the unburned gas mixture velocity.

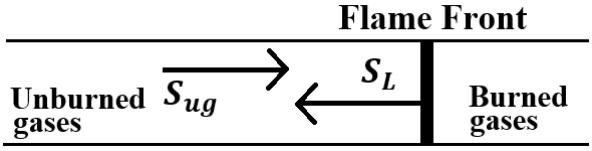

Figure 1.2: Description of laminar burning velocity

1.2.2. Influences on the burning velocity

The laminar burning velocity is dependent on three initial conditions for a given gas composition. Namely, the unburned gas temperature T_u, the pressure p_u and the equivalence ratio ϕ. Each of these properties is elaborated upon.

Temperature

Many researchers have studied the influence of the unburned gas temperature on the laminar burning velocity. The most popular correlation resulting from literature is described in equation (1.1) [20]. This form or equivalent forms are used since 1950s.

$$S_L = S_{L0}(\frac{T}{T_0})^{\alpha} \tag{1.1}$$

In this equation, T_0 is the reference temperature and S_{L0} its corresponding burning velocity at reference conditions. α, the power exponent coefficient, varies with pressure and equivalence ratio. Experiments have shown that an increase in temperature results in an increase in burning velocity [20]. Theoretical analysis on the determination of laminar burning velocities also positively correlate the temperature with the burning velocity [1]. A higher ambient temperature result in a higher final temperature, therefore increasing the reaction rate and thus burning velocity. A higher temperature also results in greater dissociation, thus a greater concentration of radicals to diffuse back. This increases the conduction of temperature in the preheating zone, and therefore resulting in a faster velocity.

Pressure

Researchers have also studied the effect of pressure on the laminar burning velocity. Measurements in studies are often interpreted using empirical power-law pressure dependence, as described in equation (1.2).

$$S_L = S_{L0}(\frac{P}{P_0})^{\beta} \tag{1.2}$$

In this equation, P_0 is the reference pressure and S_{L0} its corresponding burning velocity at reference conditions. β, the power exponent coefficient, varies with temperature and equivalence ratio [21]. The first theoretical analysis by Mallard and Le Chatelier [1] showed that the pressure depends inversely on the laminar burning velocity. The velocity declining with pressure would appear to be counter-intuitive at first. However, the thermal diffusivity also depends on the pressure, which it is inversely proportional to. Thus the effect of the pressure on the thermal diffusivity overrides the effect of the pressure on the reaction rate and the energy release rate, affecting the temperature and thus the burning velocity.

Equivalence ratio

A mixture is called stoichiometric when the mixture contains the exact amount of fuel and oxider, for all the reactants to be consumed to form products after combustion. The stoichiometric mixture is calculated by balancing the reaction equation. An example is given in equation (1.3), which is the balancing of a methane-air mixture. Here the air is assumed to consists of 21% oxygen and 79% nitrogen, volumetrically.

$$CH_4 + 2(O_2 + \frac{79}{21}N_2) -> 1CO_2 + 2H_2O + 7.52N_2 \tag{1.3}$$

The numbers before the elements are called the reaction stoichiometric coefficients. In the above equation one can deduce that for 1 mol of methane, 9.52 mol of air is needed for a stoichiometric mixture. Combustion stoichiometry for general hydrocarbons, expressed as $C_\alpha H_\beta O_\gamma$, with air is given in equation (1.4).

$$C_\alpha H_\beta O_\gamma + (\alpha + \frac{\beta}{4} - \frac{\gamma}{2})(O_2 + 3.76N_2 -> \alpha CO_2 + \frac{\beta}{2}H_2O + (\alpha + \frac{\beta}{4} - \frac{\gamma}{2})N_2 \tag{1.4}$$

In reality, mixtures are often not stoichiometric. The mixture is called lean when there is a more air than the stoichiometric amount, and called rich vice versa. It is therefore convenient to describe the mixture with the fuel-air ratio, FAR or f, given in equation 1.5.

$$f = \frac{m_f}{m_a} \tag{1.5}$$

By normalizing the actual FAR with the stoichiometric FAR, we obtain the equivalence ratio, given in equation 1.6.

$$\phi = \frac{f}{f_s} \tag{1.6}$$

The subscript s indicates that the value is at the stoichiometric condition. When it is higher than 1, the mixture is described as rich, lower than 1 is described as lean and a value of 1 corresponds to a stoichiometric mixture. The effect of the equivalence ratio on the laminar burning velocity is primarily due to its effect on the temperature. It is therefore expected that the maximum laminar burning velocity is obtained at the same equivalence ratio for the maximum temperature.

The composition of natural gas is needed to determine the corresponding mass flows for each equivalence ratio. This depends on the geographical location the natural gas is obtained. The composition of Dutch natural gas is given in table 1.1.

Table 1.1: Volumetric fractions Dutch natural Gas

Species	Volumetric fraction [%]
CH_4	81.3
C_2H_6	2.9
C_3H_8	0.4
C_4H_{10}	0.2
N_2	14.3
CO_2	0.9

1.2.3. Flame stretch

The description previously given of a premixed flame, is based on the classical model involving the steady propagation of an adiabatic, one-dimensional planar flame. This flame is characterized by a final adiabatic flame temperature, and a laminar adiabatic burning velocity. Practical flame however seldom behave in this idealized manner. In realistic situations, the flame front can be curved and non-stationary, while the upstream flow can be non-uniform. A flame experiencing these aerodynamic influences is called a stretched flame.

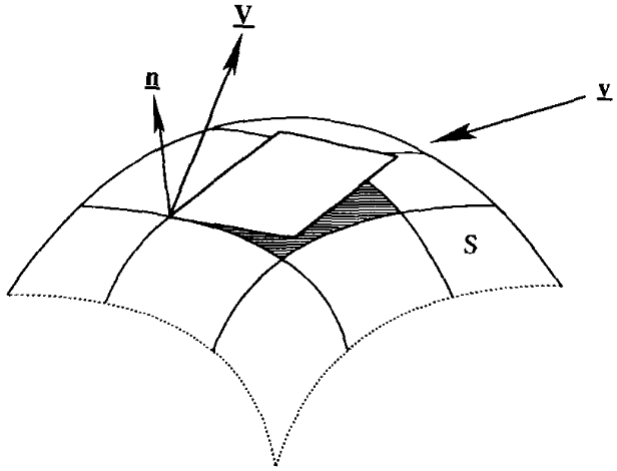

Figure 1.3: Arbitrary surface S within flame structure, with velocity V and unit normal vector n in a flow field with velocity v [2]

An arbitrary surface, s, is defined within the flame structure, shown in figure 1.3 [2].

The surface has a velocity V, while the flow has a velocity v. The general definition of the stretch rate at any point on this surface is given in equation 1.7.

$$K = \frac{1}{A}\frac{dA}{dt} \tag{1.7}$$

This is the Lagrangian time derivative of the logarithm of the area A of an infinitesimal element on the surface [22]. The boundary of this element moves tangentially along the surface at the local tangential component of the fluid velocity. The stretch rate K has the unit of sec^{-1}. This expression contains various factors that contribute to the influence of stretch. With equation 1.7, it can be shown that the stretch can be expressed as equation 1.8 in terms of the flow variables [23–25].

$$K = \nabla_t \cdot v_t + (V \cdot n(\nabla \cdot n) \tag{1.8}$$

Here, ∇_t (the divergence) and v_t are the tangential components of ∇ and v evaluated at the surface. The unit normal vector of the surface is pointing in the direction of the unburned gas, and is denoted with n. This equation embodies the effects of two sources of stretch the flame can be subjected to. The first term represents the influence of flow non-uniformity along the flame surface. This term embodies the effects due to the flame curvature and the effects due to flow nonconformity. The second term in equation 1.8 embodies the stretch experienced by a non-stationary flame. These three effects can be separately referred to as aerodynamic straining, flame curvature and flame motion.

The stretch rate K can be non-dimensionalized by the characteristic reaction time $\frac{\delta_u}{S_{L,u}}$. Here, $S_{L,u}$ and δ_u are the laminar burning velocity and the flame thickness to an unstretched flame respectively. This results in the Karlovitz number as shown in equation 1.9.

$$Ka = \frac{\delta_u}{S_{L,u}}K \tag{1.9}$$

The response of the flame stretch on the flame structure, particularly the burning velocity, is elaborated upon. The response has been found to strongly affect mixtures with unequal species and thermal diffusivities. The response for mixtures of equal diffusivities has been found to be quite subtle [15]. In an inert-abundant mixture, three diffusivities are of interest. These are the one associated with heat (D_T), the deficient reactant (D_i) and the excess reactant (D_j). Two interpretations of the effects of different diffusivities can be conducted from these three variables. The first one is for off-stoichiometric mixtures, by comparing D_T with D_i. This is also called the Lewis number (Le = $\frac{D_T}{D_i}$). The second is for near-stoichiometric situations, termed the preferential diffusion, by comparing D_i with D_j ($\frac{D_i}{D_j}$). The

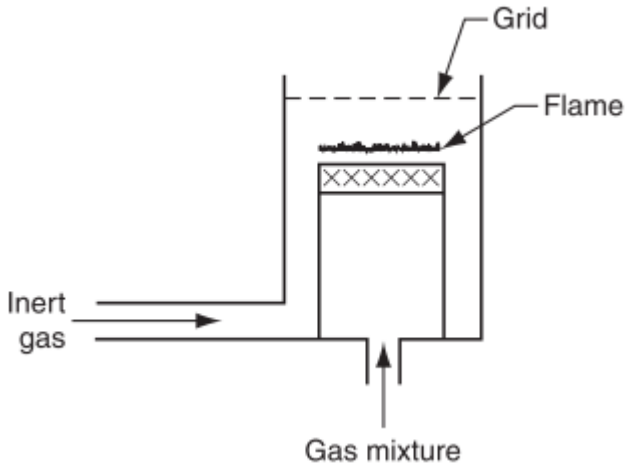

Figure 1.4: Flat flame burner illustration [1]

general phenomena related to unequal diffusion rates is termed as nonequidiffusion effects. Stretched premixed flames can thus exhibit different behaviour, depending on the positive/negative stretch and the imbalance of the thermal diffusivities. In later sections this is elaborated upon for specific flame configurations.

1.2.4. Turbulent combustion

Most practical combustion devices operate in flow conditions which are turbulent. Turbulence is favorable because it increases the mass consumption rate of the mixture to values much greater than those in laminar flames. The ratio between the turbulent and laminar burning velocity, $\frac{S_t}{S_L}$, is shown to increase almost linearly with the ratio $\frac{u'}{S_L}$, for low turbulent velocities [26]. u' is the root-mean-square of the turbulent velocity, and increases with increasing turbulence. The laminar burning velocity is also an essential parameter in the evaluation of turbulent premixed combustion models [27].

1.3. Measurement of the laminar burning velocity

Several experimental methods are available to determine the laminar burning velocity. This section presents a general description of the methods that have received considerable attention. These are the flat burner method, spherical flame method, counterflow method and the Bunsen burner method. The Bunsen burner method, which is the method of choice for this thesis, is described in detail in a later chapter.

1.3.1. Flat burner method

This method, which was developed by Powling and Edgerton, provides a close approximation to the ideal laminar burning velocity [28]. The only downside is that its limited to low burning velocities in the range of 0.15 - 0.2 m/s. A flat flame is created by placing either a porous metal disk or series of small tubes at the exit of a large flow tube. The flow is ignited with a high unburned gas velocity, and then adjusted until a flat flame is created. Having a too high unburned gas velocity results in a flame cone, and a too low velocity results in flashback. The area of the flame is measured with optical diagnostics in order to determine the laminar burning velocity. In order to accurately define the edges of the flame, an inert gas is used flowing around the burner. An illustration of this method is shown in figure 1.4. [1]. A grid is used to control the efflux of burned gases, in order to obtain a more stable flame.

1.3.2. Spherical flame method

Unlike the previous method, the spherical flame method doesn't create a stationary flame [2]. In this method, a closed constant volume is filled with the gas mixture. The mixture is ignited in the centre. A

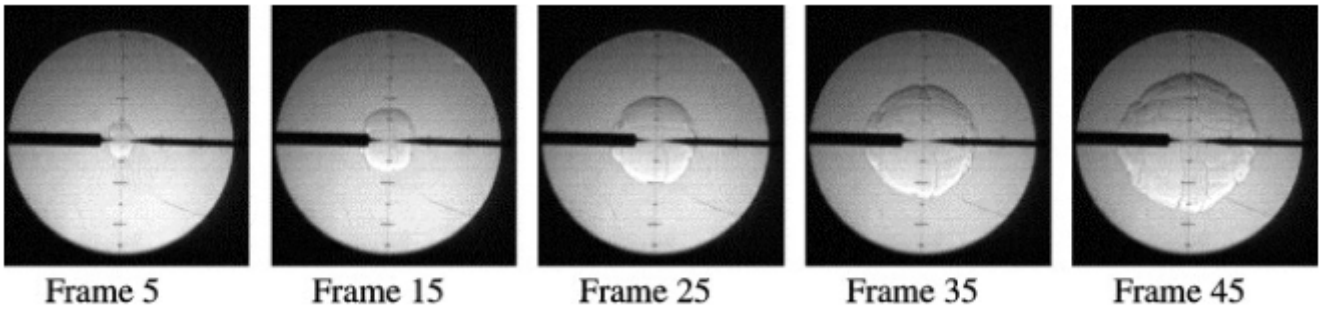

Figure 1.5: Schlieren images of an expanding hydrogen flame in a closed vessel [3]

spherically expanding flame is created travelling to the outer walls. The growth of the flame front along the radius is followed by some photographic means. The laminar burning velocity can then be derived from the radius of the flame as a function of time. Figure 1.5 shows typical results of the spherical flame method, in which the expansion of a hydrogen flame is observed [3]. With this method, the stretch rate can be calculated from the rate of change of the flame radius. This is then extrapolated to zero stretch to obtain the unstretched burning velocity. The primary limitation of this technique is the difficulty to measure flames with relatively high reactant temperature.

1.3.3. Counterflow method

In the counterflow method, two counterflowing nozzles are used to stabilize the flame [29]. The advantage of this method is that it does not suffer from heat losses to the burner, since there is no interaction with a burner rim. These flames are stretched due to the straining due to the gases that need to flow to the side. The distance between the outlet nozzles determine the strain rate. By repeating the experiment for different nozzle distances, a correlation between the laminar burning velocity and strain rate can be obtained. This can be extrapolated to obtain the unstretched laminar burning velocty.

1.3.4. Bunsen burner method

Bunsen burner flames have been extensively studied and most earlier laminar burning velocity data available have used this method to obtain a stationary flame for laminar burning velocity measurements. One of the main reasons is that it is inexpensive, versatile and easy to use. with this method, premixed gas flows up a cylindrical tube, which is long enough to ensure laminar flow, which happens to be around 50 times the tube diameter [30]. The flame can be assumed to be axisymmetric and conical in shape. The exit of the burner can either be a tube or a nozzle. Nozzle burners ensure a more uniform velocity distribution, which will lead to the sides of the cone being more straight. Two methods can be used to determine the laminar burning velocity with the Bunsen flame. These are the semi-cone angle method and the mass conservation method.

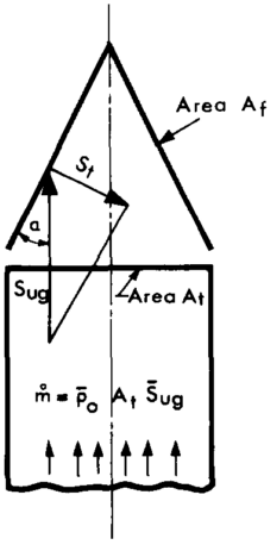

Figure 1.6: Flame cone geometry [4]

The semi-cone angle method relies on the conical shape of the Bunsen flame. The spatial velocity is 0 for a Bunsen flame, since it is a stationary flame front. This results in the burning velocity being equal to the normal component of the unburned gas velocity. This is schematically shown in figure 1.6. The corresponding equation

is given in 1.10, with S_t being the burning velocity, α the flame cone angle, and S_{ug} the unburned gas velocity. S_{ug} is replaced with U_0, which is the bulk velocity, evaluated from the burner input mass flow rate and burner exit area. This is only valid for a uniform velocity distribution. The drawback however is that the velocity distribution is rarely ever perfectly uniform, even for nozzle burners. This results in flames that are not perfectly straight-sided. The angle has to be carefully determined in those cases [6]. Particle image velocimetry can also used to circumvent this drawback. With PIV, the total velocity field is obtained. The laminar burning velocity can then be obtained with the semi-cone angle method at a specific location on the flame front.

$$S_L = S_{ug} Sin\alpha = U_0 sin\alpha \tag{1.10}$$

The second method is the mass conservation method. Here, the mass conservation balance is used, by assuming that the burning velocity is the same over the entire surface of the flame. Equation 1.11 shows the mass conservation being applied between the outlet nozzle and the flame front, with $\dot{Q}$ being the total volumetric flow rate of the unburned gas mixture. subscript u stands for the unburned gas and A_f is the total area of the flame front. The flame front area is obtained by photographic means, for example by capturing the chemiluminescence of the OH* radicals emitted from the flame. These techniques are elaborated upon later on in this thesis.

$$\rho_u S_L A_f = \rho_u \dot{Q} -> S_L = \frac{\dot{Q}}{A_f} \tag{1.11}$$

1.4. Scientific background

Many studies have been conducted about the measurements of laminar burning velocities of various hydrocarbons present on natural gas. The laminar burning velocity of natural gas depends on the composition of the hydrocarbons and other elements. The most common hydrocarbons in natural gas are methane, ethane, propane and butane. These are all gaseous at atmospheric conditions. Methane is the gas for which the laminar burning velocity has been studied the most, since it is a major compound in natural gas [31–37]. Laminar burning velocity is less studied for ethane [33, 37–42] and propane [31, 33, 38–40, 43, 44] but still have a significant impact on the burning velocity of natural gas. Butane is the least studied [44–46].

Methane has the lowest laminar burning velocity of the four hydrocarbons mentioned above according to the literature. The heat flux method shows that the maximum laminar burning velocity is about 38 cm/s, obtained for an equivalence ratio of 1.1 [47]. Ethane has the highest burning velocity, with a maximum of 42 cm/s for an equivalence ratio of 1.1. The propane laminar burning velocity profile is located between that of methane and ethane, with an maximum of 40 cm/s at equivalence ratio 1.1. The butane profile is located between that of methane and propane, with an maximum of 39 cm/s, obtained for an equivalence ratio of 1.05.

Studies can be found in literature regarding hydrogen addition to hydrocarbons and natural gas. Huang has studied the laminar burning velocity of Chinese natural gas, enriched with hydrogen from 0% to 100% [48]. Measurements have been done for methane enriched with hydrogen (10% to 50%) using the counterflow-flame method [49]. Halter et al [50] has studied methane enriched with 10% and 20% hydrogen, and Hu et al [51] for enrichment ranging from 0% to 100%. Both these studies used the combustion bomb method. The heat flux method has been used for hydrogen enrichment up to 35% [52] and up to 40% [53].There is however a lack of measurements regarding DNG laminar burning velocity measurements, as well as for DNG hydrogen mixtures.

The Bunsen burner method has been used extensively throughout the history of laminar burning velocity measurements. One of the main reasons is that it is inexpensive, versatile and easy to use. It should also give a close approximation to the unstretched laminar burning velocity [54]. The literature lacks studies in which PIV is applied for laminar burning velocity measurements. Only one study has been done using this technique [55]. It however measured for only 4 different conditions, and did not use a different measurement technique simultaneously as a comparison.

1.5. Present work and the research objective

The literature contains a wide range of laminar burning velocity measurements for unconventional fuel blends. It however lacks measurements for natural gas with hydrogen addition, and specifically for Dutch natural gas. The primary goal of this thesis is therefore the characterization of Dutch natural gas with hydrogen addition by measuring the laminar burning velocity.

The measurements are performed with a Bunsen burner method. The laminar burning velocity is measured in two ways. The first is by using the mass conservation method, by capturing the flame front with the OH* chemiluminescence. The second technique is by capturing the whole velocity field with PIV, and then applying the semi-cone angle method. The secondary goal of this thesis is to understand the performance of PIV for laminar burning velocity measurements, in comparison with OH* chemiluminescence.

There are no DNG laminar burning velocity measurements found in the literature to compare to the results in this work. In order to do this comparison as means of validating the OH*-chemiluminescence methodology, 100% hydrogen laminar burning velocity measurements are performed. This gas mixture is chosen since it has been extensively measured in the literature. The measurements are finally used to verify the performance of leading chemical kinetic mechanisms. The tool used for these computations is CANTERA and will be elaborated upon in a later chapter [56].

The research objective can thus be summarized in the following three points:

- *Characterize Dutch natural gas with hydrogen addition mixtures by measuring the laminar burning velocity*
- *Understand the performance of PIV for laminar burning velocity measurements in comparison with OH*-chemiluminescence*
- *Verify the performance of existing chemical kinetic mechanisms.*

1.6. Thesis outline

The report is outlined as follows. In the next chapter, the measurement techniques used for the experiments are explained in further detail. Chapter 3 will discuss the approach taken for this research. The numerical modelling is elaborated upon and the design of the Bunsen burner is explained. Then the experimental setup is presented together with the methodology for the post-processing of the data. After that, the uncertainties relating to the experimental measurements is elaborated upon. In chapter 4 the experimental and numerical results are presented and discussed. Finally, in chapter 5, the conclusions and future recommendations are presented.

2

Bunsen burner method

This research applies two different measurement techniques to a Bunsen flame. Namely, measuring the laminar burning velocity by capturing the OH*-chemiluminescence and by obtaining the velocity field with PIV. In this chapter, a detailed description of these two techniques is given.

2.1. Bunsen burner method

Previously, the laminar burning velocity was expressed together with the spatial and unburned gas velocity, as shown in equation (2.1).

$$S_s = S_L + S_u \tag{2.1}$$

The methods for determining the laminar burning velocity fall into two categories. Namely, one where the flame front is stationary, and one which moves with respect to a fixed point, which is usually the ignition point. For stationary flame fronts, the spatial velocity is 0, which results in $S_L = -S_u$. The Bunsen flame produces such a stationary flame. The Bunsen burner does have a couple of disadvantages. These are summarized as the following [4]:

- It lacks uniformity of the burning velocity, due to the nonuniform velocity distribution of the unburned gaseous mixture. This is particularly visible near the burner rim and at the flame tip. This could be improved by having a nozzle burner.
- The difficulty to establish the temperature profile of the unburned gas mixture. This is an essential parameter since the burning velocity depends on it.
- The non-adiabatic nature of the flame, especially near the base of the cone due to heat losses to the rim.
- Particularly for rich mixtures, air entrainment into the flame-cone base. This affects the equivalence ratio and could lead to instabilities.
- Distortion of the flame cone due to the flame thrust. These stretch effects increase with increasing unburned gas velocity.

It however still remains an acceptable method to determine the flame geometry and gives accurate approximations of the unstretched laminar burning velocity [30]. Two methods can be used to determine the laminar burning velocity with the Bunsen flame. These are the semi-cone angle method and the mass conservation method. These two methods are elaborated upon in the next sections.

2.2. Mass conservation method

In this method, the mass conservation is applied between the flame front and the exit of the burner. This gives the average laminar burning velocity of the whole flame front. The mass flow rate over the flame front is given in equation (2.2).

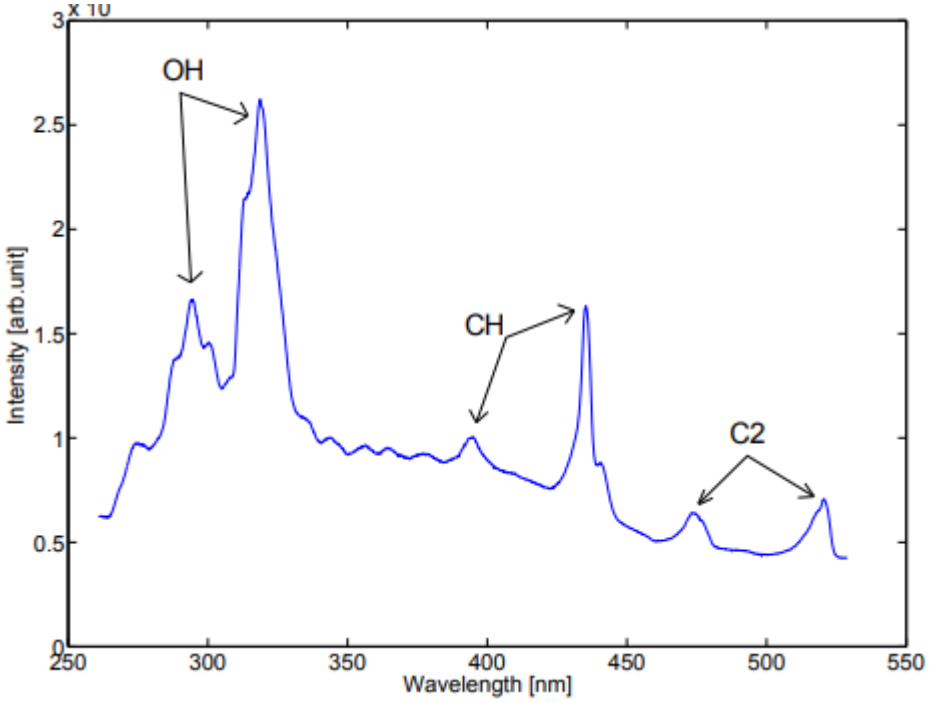

Figure 2.1: Typical emission spectrum of a Danish natural gas/air premixed flame (ϕ = 1.1, p = 1 bar) [5].

$$\dot{m} = S_b \rho_b A_b \tag{2.2}$$

Where S_b is the burning velocity of the burned gases, ρ_b the density of the burned gases, and A_b the surface area of the flame front. According to the mass balance, the burned and unburned mass flux should be equal, as stated in equation (2.3) The laminar burning velocity is relative to the unburned gas mixture, therefore S_u is equal to S_L.

$$S_b \rho_b = S_L \rho_u \tag{2.3}$$

From equation (2.2) and (2.3), equation (2.4) is obtained.

$$S_u = \frac{\dot{m}}{\rho_u A_b} = \frac{\dot{Q}}{A_b} \tag{2.4}$$

Here, $\dot{Q}$ is the volumetric flow rate of the unburned mixture. The volumetric flow rate is an input parameter for a given flame. The flame front area A_b, from now on denoted as A_f, has to be obtained. Several methods are available to observe the flame. The two most prominent ones are using Schlieren imaging and the flame chemiluminescence. Schlieren imaging visualizes the density variations of the flame. It measures the density gradient, which has the greatest value around the point of inflection on the temperature curve of the flame front. It relies on the fact that when light rays pass through the flame, they have a different index of refraction due to the density differences. The definition of Chemiluminescence is the emission of light due to chemical reactions, which is captured to obtain the flame front. This will be further elaborated upon in the next section.

2.2.1. Chemiluminescence

The definition of chemiluminescence is the emission of light due to chemical reactions. In the flame front, a number of species are created in the excited state due to chemical reactions. The de-excitation of these species results in the emission of a photon of a certain wavelength. In the UV and visible spectrum for hydrocarbons, the major radical radiation comes from OH^*, CH_4^* and C_2^* [57]. Figure 2.1 shows a typical emission spectrum for natural gas. The subscript * implies that the radicals are in an excited state.

OH* emits radiation primarily around 283, 306 and 309 nm, which is located in the ultraviolet range [58]. No shielding from visible light is required since daylight doesn't affect the signal. OH* generation can be modeled by the following reactions [58]:

$$O + H + M -> OH^* + M \tag{2.5}$$

$$CH + O_2 -> CO + OH^* \tag{2.6}$$

$$OH + M -> OH^* + M \tag{2.7}$$

Here M is any element that can be used as a catalyst. CH^* emits radiation around 390 and 431 nm. It is formed by the following reaction mechanism:

$$C_2 + OH -> CO + CH^* \tag{2.8}$$

$$O + C_2H -> CH^* + CO \tag{2.9}$$

$$O_2 + C_2H -> CH^* + CO_2 \tag{2.10}$$

CH^* is highly dependent on the flame temperature. It is usually used in flame studies as in indicator of temperature. C_2^* has the strongest presence around 516 nm. It has the disadvantage that it is not present in the lean region. The reaction mechanism for C_2^* is given by:

$$CH_2 + C -> C_2^* + H_2 \tag{2.11}$$

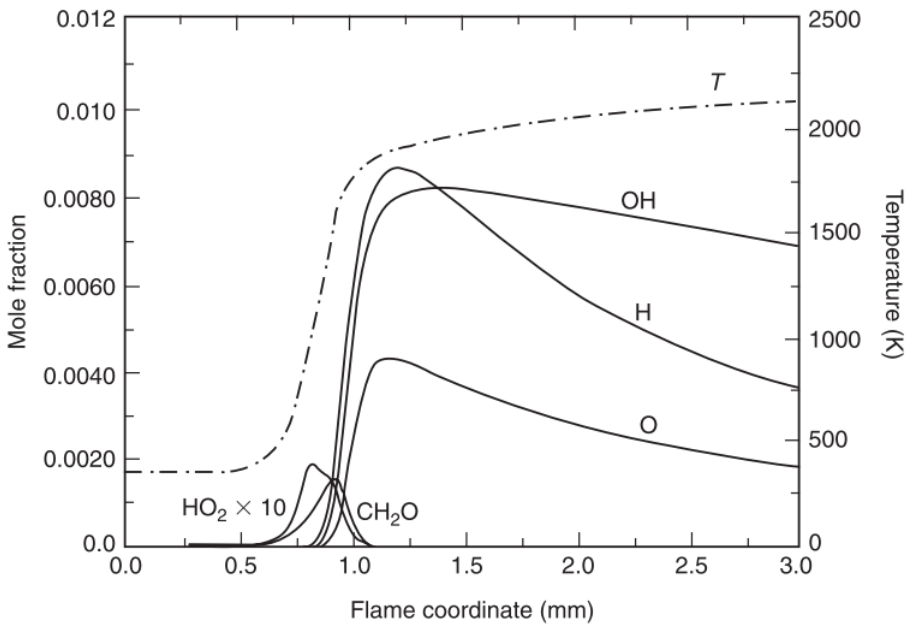

Figure 2.2: Radical distribution for methane/air flame at stoichiometry (p = 1 atm T = 298K [1]

Chemiluminescence is often used in the detection of the flame front. A CCD camera equipped with an optical filter around a certain wavelength is pointed at the flame. For OH*-chemiluminescence, a filter around 309 nm is placed. Figure 2.2 shows the OH distribution throughout the flame front. The Chemiluminescence technique will capture the flame-front at the location of maximum OH* intensity. This research will use the OH*-chemiluminescence as means for capturing the flame front for the reasons mentioned above. Using OH*-chemiluminescence is also beneficial since hydrogen addition is researched, which contains no carbon atom. The measurement of the laminar burning velocity with

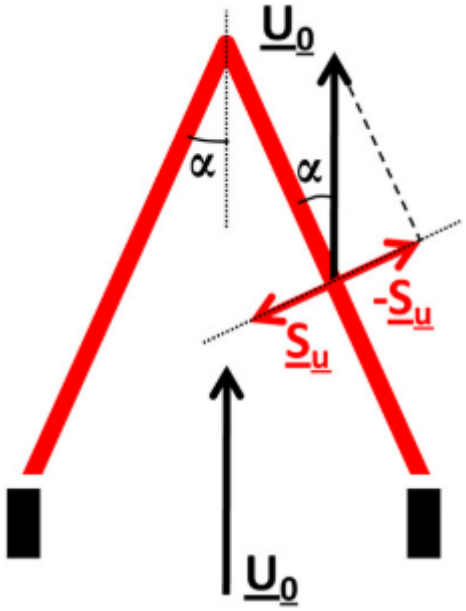

Figure 2.3: Schematic of the cone-angle methodology [6]

OH*-chemiluminescence is a passive technique. This entails that the all 3D information contained in the flame will be captured by the camera. Each pixel shows the line of sight information through the entire flame.

2.3. Semi-cone angle method

The semi-cone angle method uses the flame geometry to calculate the laminar burning velocity. This method is particularly convenient for straight-sided cones. These require an aerodynamically contoured nozzle. When considering the unburned gas velocity as uniform, the laminar burning velocity can be calculated as follows (figure 2.3):

$$cos(\frac{\pi}{2} - \alpha) = \frac{S_u}{U_o} -> S_u = U_o sin(\alpha) \tag{2.12}$$

Here, U_o is the unburned gas bulk velocity, α the half cone angle, and S_u the laminar burning velocity relative to the unburned gas, which equals S_L. The simplicity of this method is counterbalanced since flames are rarely perfectly straight-sided, even with contoured nozzles. Boundary layer effects alter the evolution of both U_o and α along the flame border. The laminar burning velocity is also not consistent over the whole border, due to stretch effects and heat losses to the rim. A way to circumvent these limitations is by using Particle image velocimetry, which gives the whole velocity field of the flame. Therefore the velocity vector and half cone angle can be locally extracted on the flame front, instead of a global parameter. PIV is elaborated upon in the next section.

2.3.1. PIV

PIV stands for particle image velocimetry. This method visualizes the velocity field, from which the laminar burning velocity can be deduced at each location. The gaseous mixture is seeded with particles, which are being illuminated. From the trajectories of these particles, the velocities and directions can be determined. PIV is an active technique in which a 2D snapshot of the flame is taken. Therefore the image is not distorted by the 3-dimensional nature of the flame.

The seeding particles must be sufficiently small in order to accurately follow for the flow, but large enough to scatter sufficient light from the incident laser. The refractive index of the particles should differ from that of the fluid so that only they are reflected from the laser sheet. Particle diameter should be selected to be small enough to avoid quenching of the flame due to them being inert. It

should also have a sufficient diameter for the later sheet to accurately visualize the velocity field, and be heat-resistant if used for flames.

A laser is used to generate two light sheets to illuminate the particles in the flow. A series of optical lenses are used to transform the point laser into a collimated sheet. Two pulses are generated with a certain δT in between. From this δT, the displacement of each particle can be deduced, and thus the velocity field can be determined. This is then measured by a CCD camera fitted with an optical bandpass filter, in order to minimize the flame luminosity.

Few studies have been performed in determining the laminar burning with PIV measurements. Kurtulus et al. used the PIV technique to determine the instantaneous flame front position and flow velocities [55]. The aim of the study was to contribute to the characterization of methane-air premixed laminar flames. This was done at two different equivalence ratios without a different measurement technique at a comparison. The study used aluminum oxide particles in order to capture the velocity field and flame front position. This research will use PIV to determine the whole velocity field of the flame. The location of the flame front can be determined where the velocity increases rapidly due to the thermal expansion of the combustion process. The laminar burning velocity can then be determined at specific points over the flame front. The experimental setup and the methodology for analyzing the PIV data will be elaborated upon in a later chapter.

3

Research methodology

In this chapter, the methodology for this research is explained in detail. Firstly, the methodology used for the numerical modeling is explained. the design of the Bunsen burners and the assigned mass flows are explained afterwards, since they require numerical simulations for their design. This is done for both DNG hydrogen mixtures and the pure hydrogen mixture used for the validation. Then, the methodology for both measurement methods, with OH*-chemiluminescence and PIV, are elaborated upon. Their experimental setup is explained as well as the data processing methodology. After that, the uncertainties related to this research are discussed.

3.1. Numerical modelling

Laminar burning velocities are predicted numerically with a chemical kinetic mechanism. These calculations are performed using a commercial kinetics software package called Cantera [56]. The numerical calculations are used in the design of the burner diameter. They are also compared to the experimental burning velocity measurements from OH*-chemiluminescence and PIV. Cantera includes a set of models to represent steady state, quesi-one- dimensional reacting flows. In order to determine the laminar burning velocity numerically, a 1D flame code is written for a freely-propagating premixed laminar flame.

The flames in Cantera are modeled in an axisymmetric stagnation flow. The solution is computed along the stagnation streamline. A similarity solution is used to reduce the three-dimension governing equations to a single dimension. The governing equations used for a steady axisymmetric stagnation flow are as follows:

$$\text{continuity:} \quad \frac{\partial \rho u}{\partial z} + 2\rho V = 0 \tag{3.1}$$

$$\text{Radial momentum:} \quad \rho u \frac{\partial V}{\partial z} + \rho V^2 = -\Lambda + \frac{\partial}{\partial z}\left(\mu \frac{\partial V}{\partial z}\right) \tag{3.2}$$

$$\text{Energy:} \quad \rho c_p u \frac{\partial T}{\partial z} = \frac{\partial}{\partial z}\left(\lambda \frac{\partial T}{\partial z}\right) - \sum_k j_k c_{p,k} \frac{\partial T}{\partial z} - \sum_k h_k W_k \dot{\omega}_k \tag{3.3}$$

$$\text{Species:} \quad \rho u \frac{\partial Y_k}{\partial z} = -\frac{\partial j_k}{\partial z} + W_k \dot{\omega}_k \tag{3.4}$$

Here, ρ is the density, u the axial velocity, v the radial velocity, V the scaled radial velocity (v/r). Λ is the eigenvalue of the pressure, μ is the dynamic viscosity, c_p the heat capacity at constant pressure, T the temperature, λ is the thermal conductivity, Y_k is the mass fraction of species k, j_k is the diffusive mass flux of species k, $c_{p,k}$ is the specific heat capacity of species k, h_k the enthalpy of species k, W_k the molecular weight of species k, and $\dot{w}_k$ is the molar production rate of species k. The tangential

velocity is assumed to be zero. The gas is modeled to behave as an ideal gas.

Cantera provides a set of transport manager classes, to compute the transport properties. Two transport models are available to choose from, namely the 'mixture-averaged' and the 'multicomponent' transport model. The 'multicomponent' formulation takes into consideration the diffusion of species k into each species j, as opposed to the 'mixture-averaged' formulation. It however exponentially increases the computational time. For this reason and because the computed laminar burning velocities with both models are within 1% of each other, the 'mixture-averaged' transport model is selected for all calculations.

For the freely propagating premixed flame, inlet boundary conditions have to be specified. These values are supplied for the temperature T_0 and the species mass fraction $Y_{k,0}$. Cantera will use a modified Newton algorithm to solve for the steady-state solution vector at each grid point in the domain. The velocity at the start of the flame, the first grid point, is then the laminar burning velocity.

In order to calculate the flame properties with Cantera, a combustion reaction mechanism for a set of species is required. Several reaction mechanisms can be found in the literature. GRI-Mech 3.0 is selected for the computations in this thesis [59]. This is an optimized mechanism designed to model natural gas combustion. This mechanism contains 325 reactions and 53 species, including the hydrocarbons present in DNG, and hydrogen.

3.2. Bunsen burner design

The goal in the design of the Bunsen burner is to achieve a stable flame cone over a wide range of equivalence ratios. The stability limits associated with a laminar Bunsen flame are the phenomena of flashback, blowoff and the onset of turbulence. First, an explanation of these phenomena are given, together with the procedure to design the burner diameter. Afterwards, the design for the hydrogen mixture burner and the DNG hydrogen mixture burner is elaborated upon.

In the introduction, an explanation for the laminar burning velocity was given. When the unburned gas mixture in a tube has the same velocity as the laminar burning velocity, the flame front is stationary. Increasing the unburned velocity results in propagation of the flame front, till it exits the tube. Increasing the unburned gas mixture further results in a conical shape, the Bunsen flame. The greater the unburned velocity, the higher the flame cone and thus the lower the flame cone angle. This happens because the velocity component normal to the flame front has to equal the laminar burning velocity. Near the burner rim, the velocity is lower than the centre, and at some point it is equal to the laminar burning velocity and anchors at that point. As the flow velocity is increased, this point moves further from the burner. At a certain point, the flame edge moves too fat outwards and outside air is entrained. The mixture is diluted, the burning velocity drops, and blowoff occurs. The opposite phenomenon is called flashback. Here the unburned gas mixture is gradually reduced, until it reaches a point in the flow field that the laminar burning velocity exceeds the unburned gas mixture. The flame will then propagate downwards.

The other stability limit which has to be accounted for is the onset of turbulence. The Reynolds number must not exceed a value of 2000 in order to obtain a fully developed laminar flow [60]. The Reynolds number is defined by equation (3.5). Where D_H is the hydraulic diameter (m), Q the volumetric flow rate ($\frac{m^3}{s}$), ν the kinematic viscosity ($\frac{m^2}{s}$) and A the cross-sectional area of the tube (m^2).

$$Re = \frac{Q D_H}{\nu A} \tag{3.5}$$

The cross-sectional area of the burner is calculated as follows:

$$A = \frac{\pi}{4} D_H^2 \tag{3.6}$$

The hydraulic diameter is defined as the wetted area of the tube, which for a circular shape, is simply the diameter (D). Experimental evidence has shown that the average unburned gas velocity

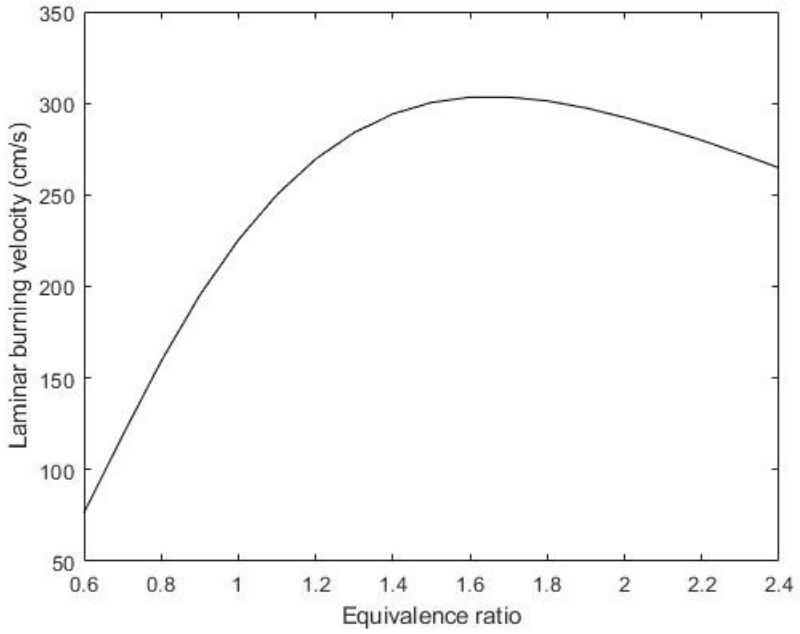

Figure 3.1: Laminar burning velocity versus equivalence ratio for hydrogen air mixtures using GRI 3.0 Mech (T = 293 K, p = 1 atm)

should be more than twice the laminar burning velocity, but less than 5 times, in order to obtain a stable Bunsen flame. Thus the following three criteria have to be met in the design of the burner:

- Reynolds number should be less than 2000
- Unburned gas velocity should be more than 2 times the laminar burning velocity
- Unburned gas velocity should be less than 5 times the laminar burning velocity

With these design criteria in mind, the two burners are designed.

3.2.1. Hydrogen burner

The laminar burning velocities are needed to determine the required burner diameter. Cantera is used to calculate the laminar burning velocities for hydrogen air mixture at ambient conditions (T = 293K and p = 1 atm). The GRI 3.0 Mech kinetic mechanism is used. These results are shown in figure 3.1.

The equivalence range of interest is between 0.8 and 2.2. The laminar burning velocities in this range are between 1.6 and 3.0 m/s. The burner diameter has to be chosen such that the bulk velocity is in the range of 6 to 8 m/s, according to the design rules for a stable conical flame.

In order to calculate for the Reynolds number, a preliminary burner diameter has to be chosen beforehand. The burner size is chosen depending on the available tubing and the sizes used in the literature. Based on these points, a 4mm burner is chosen [6] [34]. The unburned gas velocity U_0, is plotted against the Reynolds number for a 4mm burner. The kinematic viscosity however depends on the gas composition. This changes with changing equivalence ratio. The effect of the equivalence ratio on the kinematic viscosity is determined with Cantera and plotted in figure 3.2.

The kinematic viscosity increases with equivalence ratio. It is inversely proportional to the Reynolds number. Therefore, the kinematic viscosity for the lowest equivalence ratio is chosen in the computations. The Reynolds number versus the unburned gas velocity is plotted in figure 3.6. Here, the unburned gas velocity is defined as follows:

$$U_0 = \frac{Q}{A} \tag{3.7}$$

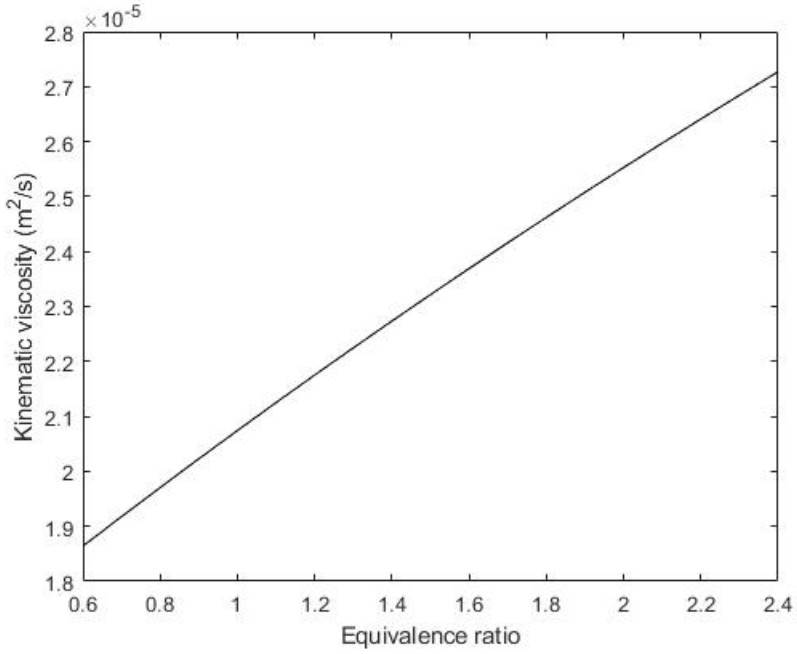

Figure 3.2: Kinematic viscosity versus equivalence ratio for hydrogen air mixtures (T = 293K and p = 1 atm)

The intersection occurs for U_0 = 9.15 m/s, which is thus the maximum allowable bulk velocity to still have laminar flow. Thus 4mm burner satisfies the laminar flow condition when operating in the velocities required to acquire a conically shaped flame (6-8 m/s). Therefore, the 4mm burner is selected for the experimental measurements for the 100% hydrogen air mixtures validation run.

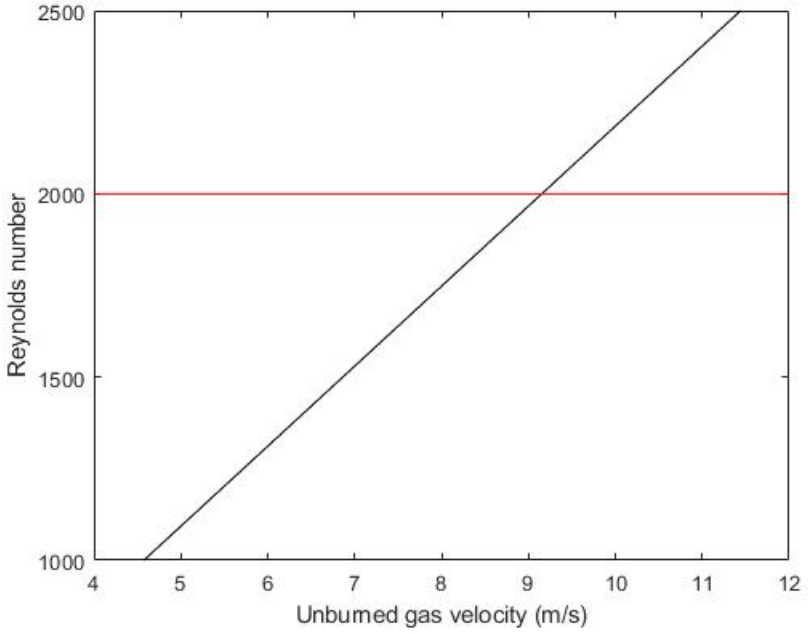

Figure 3.3: Unburned gas velocity versus Reynolds number for hydrogen air mixture at 0.8 equivalence ratio (T = 293K and p = 1 atm)

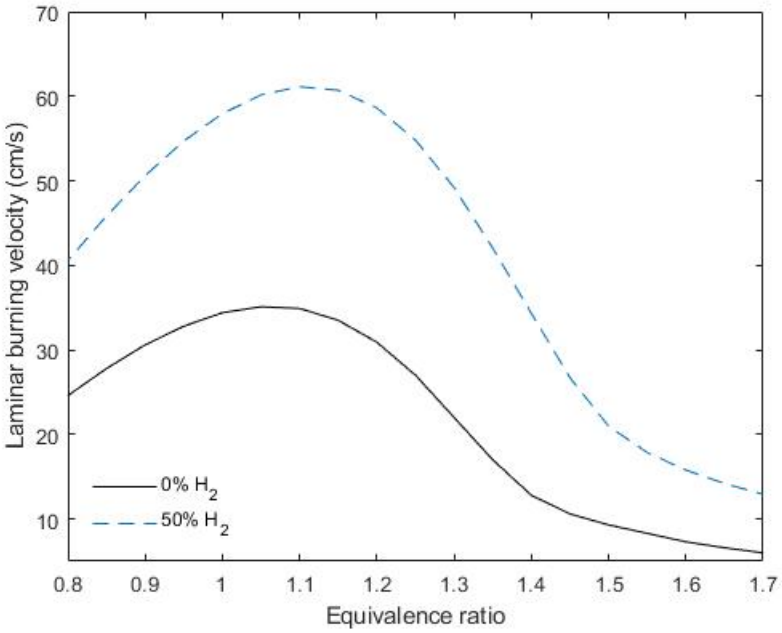

Figure 3.4: Laminar burning velocity versus equivalence ratio for DNG-hydrogen air mixtures using GRI 3.0 Mech, for 0% and 50% hydrogen addition (T = 293 K, p = 1 atm)

3.2.2. DNG-hydrogen mixture burner

The same procedure is done for the DNG-hydrogen mixture burner. The maximum volumetric hydrogen addition to DNG will be 50% in 10% increments. In the next section, this choice will be discussed in more detail in combination with the mass flow controllers. The laminar burning velocities are needed to determine the stability criteria for the DNG-hydrogen experiments. Figure 3.4 shows the laminar burning velocity versus equivalence ratio for both 0% and 50% hydrogen addition.

The maximum burning velocity is 61.2 cm/s obtained at 50% hydrogen addition. The burner diameter should thus be selected such that twice this velocity can be pushed through the tubes while still remaining on the laminar flow regime. Again a preliminary burner diameter is selected based on the available burners and documentation in the literature. Based on these points, a 12mm burner is selected [8]. The same procedure is done to determine the limits related to the Reynolds number. In this case, the kinematic viscosity also changes with hydrogen addition. These two parameters plotted against each other in figure 3.5.

The lower the hydrogen addition, the lower the kinematic viscosity. Thus the stability limit is calculated with the 100% DNG air mixture. The Reynolds number versus the unburned gas velocity is plotted in figure 3.6. The intersection occurs at a U_0 = 2.25 m/s, which is thus the maximum allowable bulk velocity to stay in the laminar flow region. This is more than the 1.2 m/s required due to the maximum laminar burning velocity of 50% hydrogen addition. The 12mm burner is therefore selected for the DNG-hydrogen mixture experiments.

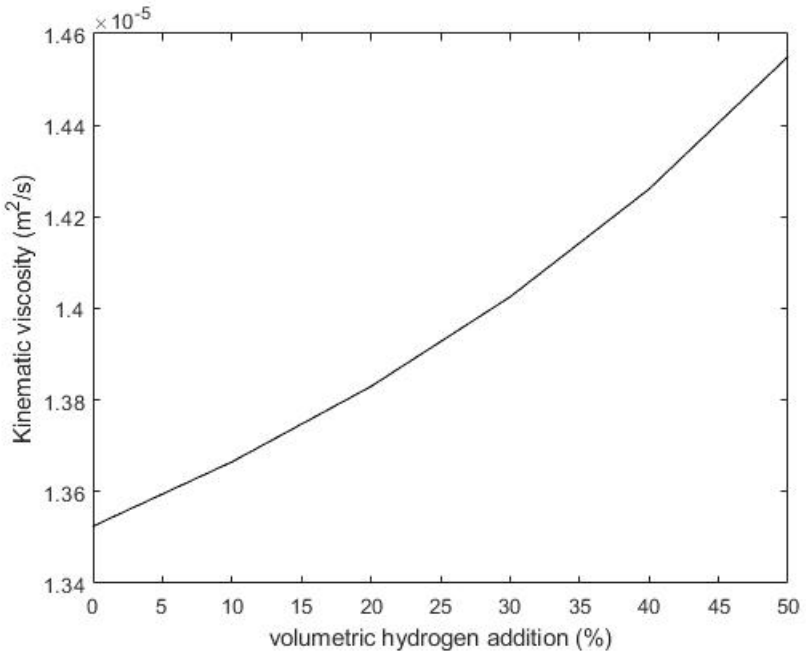

Figure 3.5: Kinematic viscosity versus volumetric hydrogen addition for DNG-hydrogen air mixtures (T = 293K and p = 1 atm)

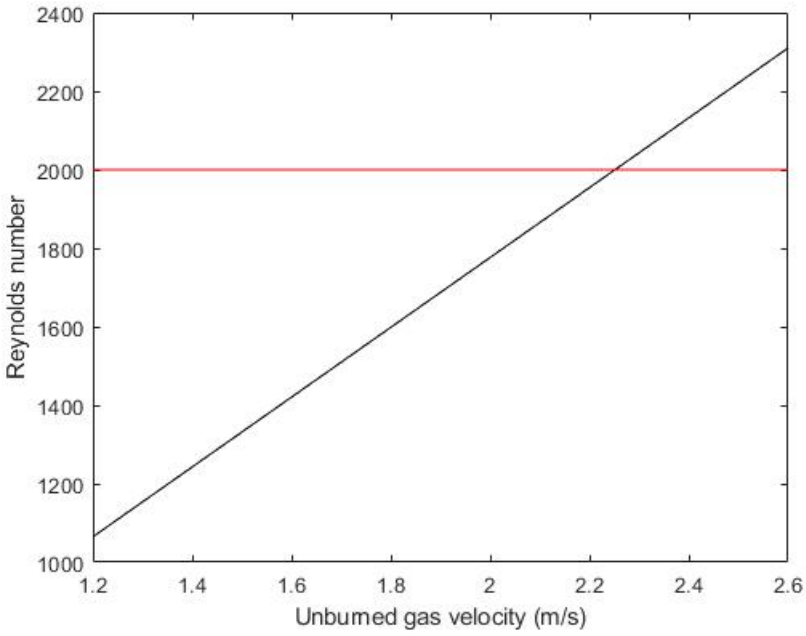

Figure 3.6: unburned gas velocity versus Reynolds number for DNG air mixture at 0.8 equivalence ratio (T = 293K and p = 1 atm)

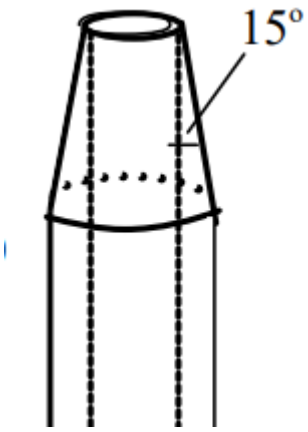

Figure 3.7: tapered burner rim 12mm burner [7]

3.2.3. Piping length and taper

The diameter for both burners are summarized in table 3.1. The burner length for both burners was chosen on the conventional 50 times the diameter criterion [7]. This is to ensure that the laminar flow is fully developed once it reaches the burner rim. Both burners comply with this criterion by being 1 meter in length each. The exit of the 12mm burner has been tapered at an angle of 15 degrees as seen in figure 3.7. A tapered tip reduces the heat losses to the burner rim [7]. However, the re-circulation at the burner rim is reduced, thus reducing the stability limit. The 4mm burner is not tapered because the required machining was not available for such a small burner.

Table 3.1: Burner diameter for DNG/hydrogen and hydrogen fuel mixture experiments

Fuel mixture	Burner diameter (mm)
DNG/hydrogen - air	12
Hydrogen - air	4

3.3. Investigated parameter range

For OH*-chemiluminescence measurements, pure hydrogen air mixtures will be investigated first in order to validate the OH*-chemiluminescence methodology. This will be done for the equivalence range 0.7 to 2.1 in steps of 0.1. Secondly, DNG-air mixtures are investigated up to 50% volumetric hydrogen addition. This is done in 10% increments. Thus for 10, 20, 30, 40 and 50% hydrogen addition. The equivalence ratio is varied between 0.8 and 1.6 in steps of 0.1. The Reynolds number is kept constant for the different hydrogen additions in order to have the same flow conditions.

PIV is a time consuming procedure for laminar burning velocity measurements. Therefore, only 12 measurement points are selected. 0, 20 and 50% hydrogen addition fuel compositions are selected. These are each measured for equivalence ratio 1 and 1.4. Each measurement is also done with 2 different Reynolds numbers, in order to investigate the effect of the bulk velocity on the laminar burning velocity measurement with PIV.

The volumetric flow rates are controlled by mass flow controllers (MFC) from Bronkhorst [61]. These mass flow controllers are specified for certain ranges expressed in normal liters per minute (l_n/min). This is the volumetric flow rates expressed for normal conditions, which is a temperature of 273.15 K and 1 atmosphere pressure. The ideal gas law can be assumed, which is given in equation (3.8). The formula shows that moles and volume are linearly correlated. Thus the same stoichiometric fractions can be used for the volumetric mass flows.

$$PV = nRT \tag{3.8}$$

Table 3.2: Volumetric flow rate controllers operational range

Volumetric flow controller	Operational range	Rd (%)	FS (%)
Hydrogen (F-201CV-20K)	0.16 l_n/min - 25 l_n/min	0.5	0.1
DNG (F-111AC-70K)	0.6 l_n/min - 30 l_n/min	0.5	0.1
Air (F-203AV-M50)	4 l_n/min - 500 l_n/min	0.5	0.1

Table 3.3: Measurement points for OH*-chemiluminescence

Fuel mixture (vol. %)	equivalence ratio range	Reynolds number	Unburned gas velocity (m/s)
Hydrogen	0.7-2.1	1750	8.0
DNG	0.8-1.6	1600	1.81
DNG-hydrogen (90/10)	0.8-1.6	1600	1.83
DNG-hydrogen (80/20)	0.8-1.6	1600	1.85
DNG-hydrogen (70/30)	0.8-1.6	1600	1.87
DNG-hydrogen (60/40)	0.8-1.6	1600	1.91
DNG-hydrogen (50/50)	0.8-1.6	1600	1.94

The accuracies of these controllers are specified as a percentage of full scale (FS) and a percentage of reading (RD). FS is relative to the maximum mass flow the controller is calibrated for. RD is relative to the actual mass flow. The hydrogen line uses the Bronkhorst F-201CV-20K. DNG uses the Bronkhorst F-111AC-70K. Air uses the Bronkhorst F-203AV-M50. The ranges and accuracies of these controllers are given in table 3.2.

The determination of the volumetric mass flows for each equivalence ratio, and thus the corresponding Reynolds number and unburned gas velocity, is constraint by the minimum value of the mass flow controllers. Taken into account these limits, a summary of the measurement points for OH*-chemiluminescence and its corresponding Reynolds number and unburned gas velocity is given in table 3.3. A summary for the 12 measurement points done with PIV is given in 3.4.

3.4. Measurement approach

In this section the experimental apparatus for both techniques is elaborated upon together with the data analyzing procedure.

3.4.1. OH*-chemiluminescence

An intensified charge-coupled device (ICCD) camera is used to record the OH* chemiluminescence emitted from the flame. The camera used is the CamRecord 600 from Optronis, which is an 24-bit ICCD camera has a 1280x1024 array, capable of 500 frames per second (fps). The camera is equipped with a f/4.5, f = 105mm Nikkon lens. The lens is equipped with a 308nm band-pass filter with a bandwidth of 2.5nm, to only capture the OH*.

The digital resolution for each image is set at 1280x720. The measurement time is set at 2 seconds

Table 3.4: Measurement points for PIV

Fuel mixture (vol. %)	equivalence ratios	Reynolds number	Unburned gas velocity (m/s)
DNG	1.0 and 1.4	1100	1.21
DNG	1.0 and 1.4	1600	1.81
DNG-hydrogen (80/20)	1.0 and 1.4	1600	1.85
DNG-hydrogen (80/20)	1.0 and 1.4	1800	1.85
DNG-hydrogen (50/50)	1.0 and 1.4	1600	1.94
DNG-hydrogen (50/50)	1.0 and 1.4	1800	2.21

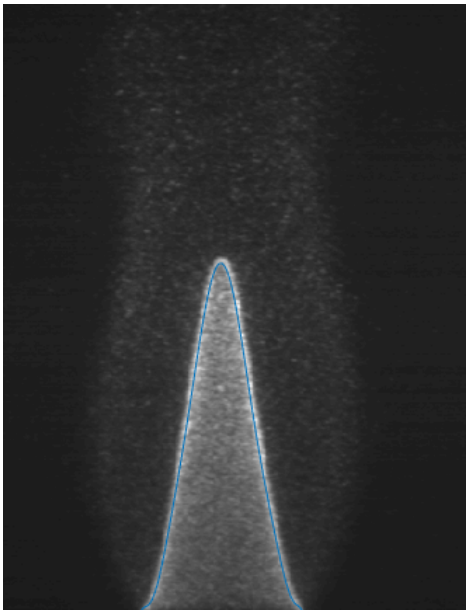

Figure 3.8: Maximum OH* intensity fitted with a 10th order polynomial.

with an image acquisition rate of 200 fps. This implies that each measurement point results in 400 images. The intensifier gain is set at 3000 with an exposure time of 2 milliseconds (2ms). These values were selected such that the maximum OH* contour could be extracted without having too much noise in the images.

Image analysis

The contour for the maximum OH* intensity has to be extracted from the acquired images in order to determine the laminar burning velocity. In order to remove noise, the average of each 4 images is taken. The average implies the average pixel value in each pixel. This results in 100 images for each measurement point.

A Matlab algorithm is written to find the contour for the maximum OH*. Along each vertical line, the location of the maximum OH* is found. A 10th order polynomial is fitted through these points. An example flame image with the polynomial plotted over the flame contour can be seen in figure 3.8.

Once the contour of the flame is determined, the flame area is calculated with equation (3.9).

$$A_f = 2\pi \int_b^a f(x)\sqrt{2 + [f'(x)]^2}dx \tag{3.9}$$

f(x) is the polynomial through the maximum OH*. The integral is integrated from a to b. Which is the one base of the flame until the flame tip, resulting in the total flame area by using the contour for one half of the flame. The integral is calculated for both halves of the flame, and the average is taken. The flame front area is then obtained in terms of pixels. This is scaled with the pixels per meter ratio to obtain the flame area in meters.

The variation of the laminar burning velocity through time is calculated for each measurement point. Figure 3.9 shows an example measurement for DNG-air mixture at 1.1 equivalence ratio. The average of the measurements is documented as the laminar burning velocity. The error margins are presented using a 95% confidence interval. The confidence interval is calculated as follows[62]:

$$[\bar{S_L} - Z\frac{\sigma}{\sqrt{n}}, \bar{S_L} + Z\frac{\sigma}{\sqrt{n}}] \tag{3.10}$$

Here, $\bar{S_L}$ is the mean laminar burning velocity, σ the standard deviation and n the sample size. The critical value Z is 1.96 for a 95% confidence interval.

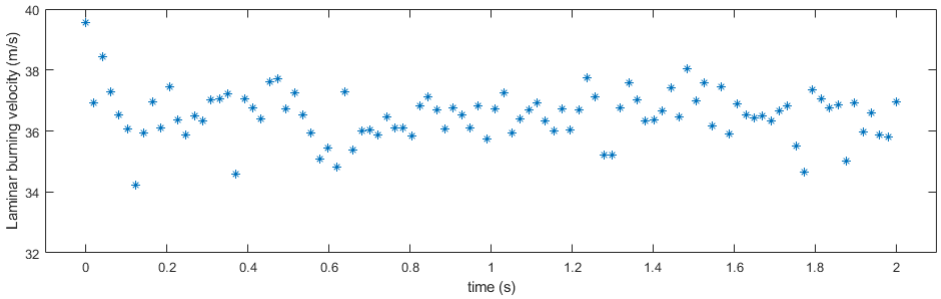

Figure 3.9: Laminar burning velocity versus time for DNG-air mixture at 1.1 equivalence ratio (T = 293K and p = 1 atm). OH*-chemiluminescence measurements taken at an acquisition rate of 200 fps for a duration of 2 seconds

3.4.2. PIV

The PIV measurements of the flow field were taken with a with a Litron Lasers NANO-L50-50PIV model. The solid particles were illuminated with a double-pulsed solid state frequency-doubled neodymium-doped yttrium aluminium garnet laser (Nd: YAG). The ouput wavelength of the laser is 532nm. The maximum output of the laser is 400mJ, with a pulse duration of 4ns. The maximum repetition rate is 50Hz. The interval between two pulses of 50 μs was selected, to allow for sufficient movement between the seeding particles, which is approximately 5 pixels. The beam is shaped into a thin laser sheet with a 3 lens setup. First, it passes a cylindrical lens with a focal length of 38.1mm and a spherical lens with a 300mm focal length.

The scattering of the seeding is captured with a Photron 675k-M3 high-speed camera. The camera records black and white with a resolution of 1024x1024 pixels and has a 12-bit ADC sensor with 20 μm pixels. The camera is equipped with a 60mm AF Micro Nikkor lens. The camera field of view was selected to be 70 x 70 mm with a resolution of 1024x1024. This results in a pixel size of 68.4 $\mu m/pixel$. The data acquisition was set at 50 Hz for a duration of 4 seconds. This results in 200 measurements.

The unburned gas mixture was seeded with aluminum oxide particles (Al_2O_3). The seeding was supplied to both the fuel and oxidizer with seeding devices. In these devices, the flow enters the bottom and creates a vortex which picks up seeding and exits at the top. A valve is regulated to determine the seeding density. The seeding density is an important parameter. Enough seeding should be present to be able to accurately trace the velocity field. It is desirable to have at least 10 particles in an interrogation window [63]. However, the seeding also influences the flame chemistry. This results in heat losses as the particles take energy away from the gas. Therefore a tradeoff between these two effects has to be made. 3.10 shows an image of the average seeding density obtained for the measurements.

DaVis software

DaVis software by LaVision was used to analyze the PIV images [64]. Each frame is split into a large number of interrogation areas for which the displacement vector is calculated. The window has to be chosen such that it is small enough to provide enough resolution of the flow field and large enough to not generate significant noise. A window size of 8 x 8 is chosen. Each measurement point consists of 200 instantaneous velocity fields, for which an example is represented in figure 3.11. The black dots are locations for which the velocity could not be calculated. The 200 consecutive images are averaged, resulting in an average velocity field and standard deviation field represented in figure 3.12 and 3.13 respectively. These fields are presented using the Matlab toolbox PIVmat [65].

Burning velocity analysis

The semi-cone angle method is used to calculate the laminar burning velocity at each location on the flame front. The first step is to determine the position of the flame front. A Matlab algorithm is written to determine the location of the flame front to be the position at which the vertical velocity component starts accelerating due to the thermal expansion of the reaction of combustion. Figure 3.14 shows the streamline along the burner that is taken in this sample calculation. Figure 3.15 shows the corresponding vertical velocity line, with the position of the flame front marked. The flame front could

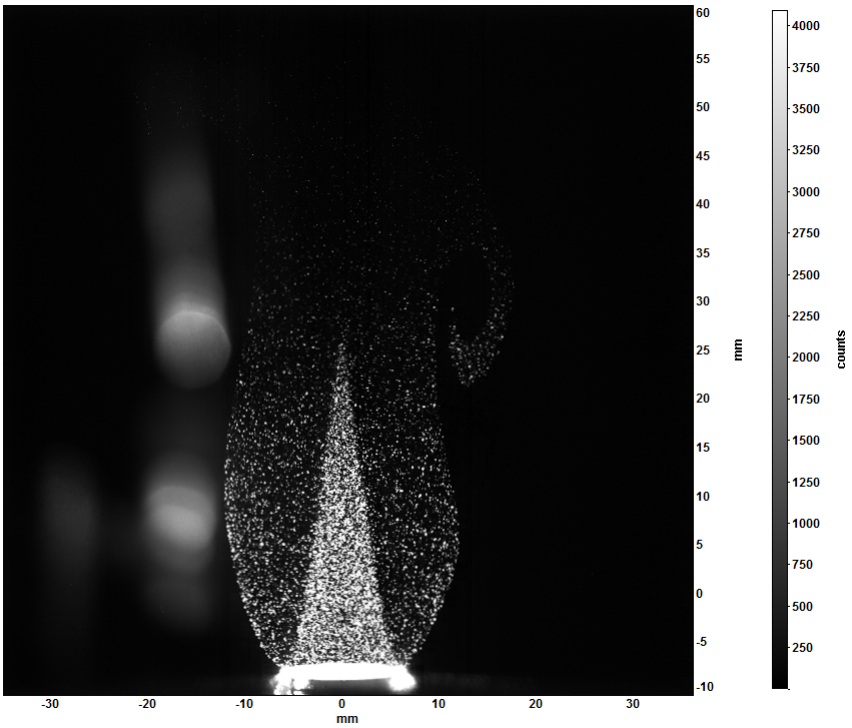

Figure 3.10: Example of instantaneous shot of Bunsen flame with seeding for DNG-hydrogen (50/50) air mixture. (T = 293 K, p = 1 atm)

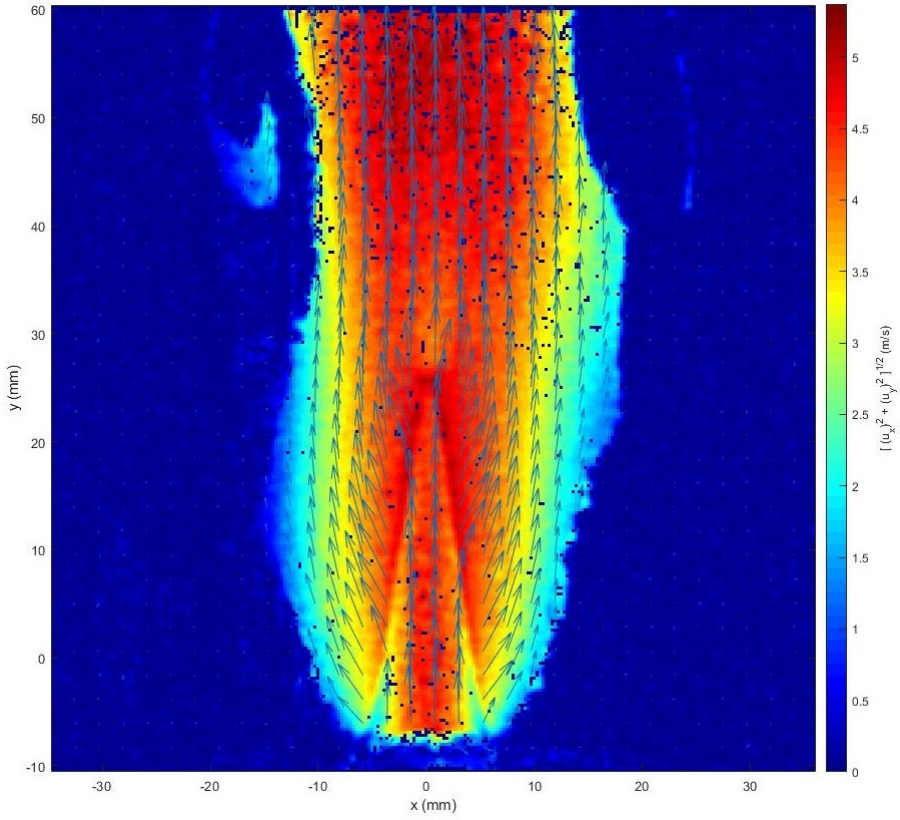

Figure 3.11: Instantaneous velocity field example for DNG-hydrogen (50/50) air mixture. (T = 293 K, p = 1 atm)

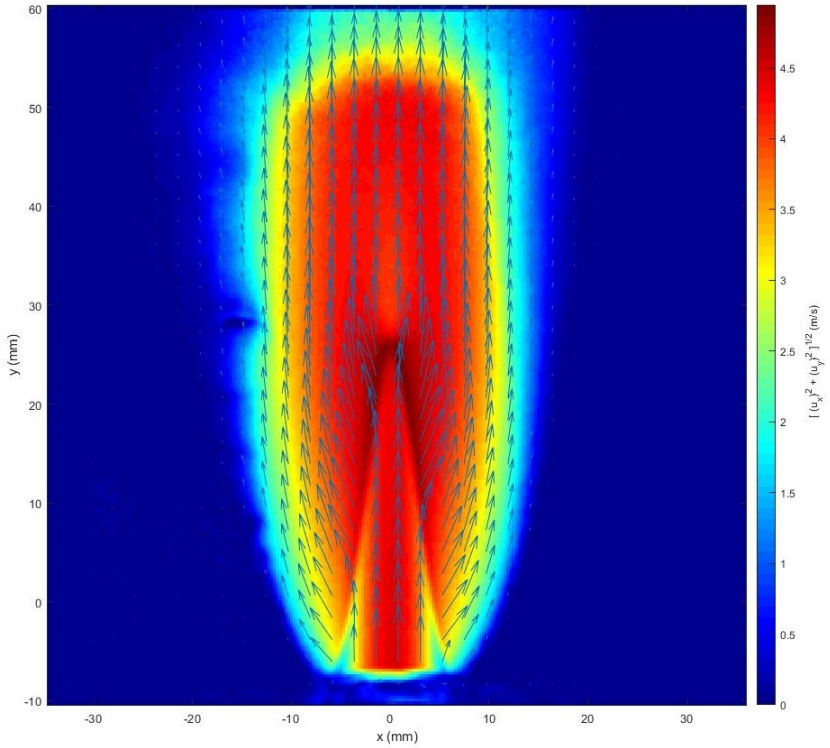

Figure 3.12: Average velocity field example for DNG-hydrogen (50/50) air mixture. (T = 293 K, p = 1 atm)

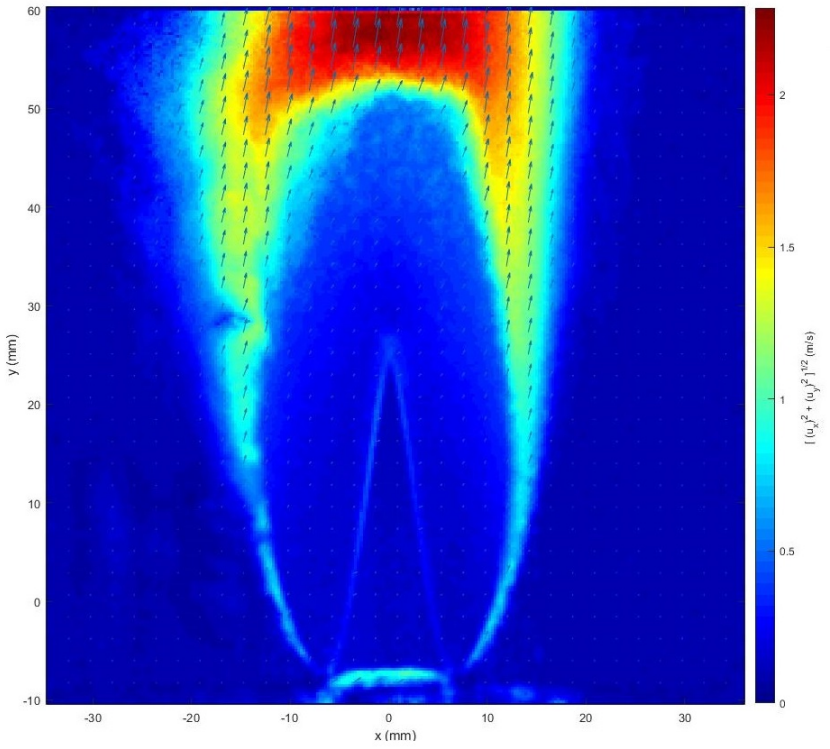

Figure 3.13: Average standard deviation field example for DNG-hydrogen (50/50) air mixture. (T = 293 K, p = 1 atm)

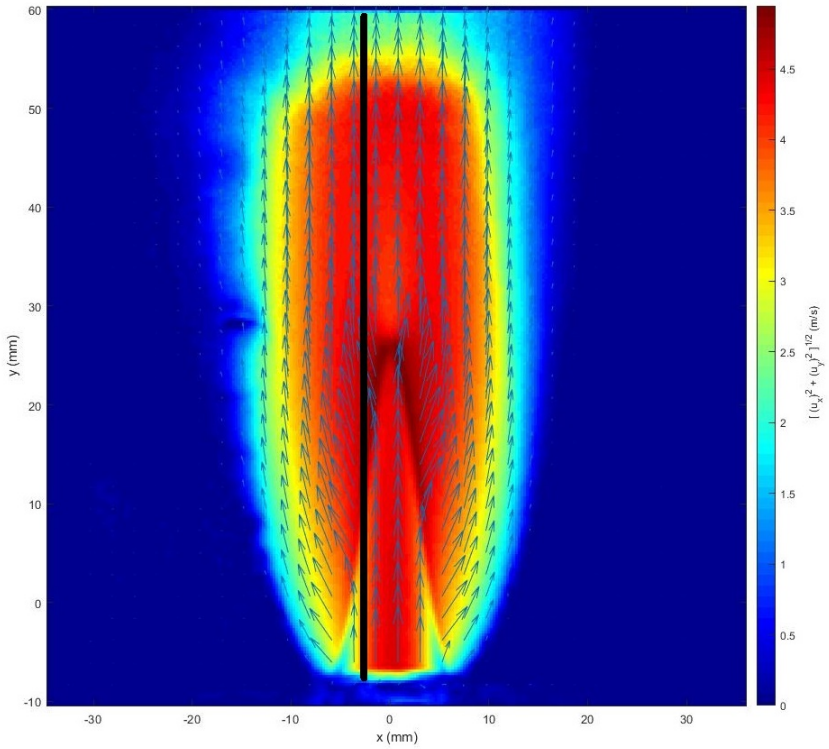

Figure 3.14: Position of evaluated streamline for DNG-hydrogen (50/50) air mixture at 2.81 mm left from the burner centre. (T = 293 K, p = 1 atm)

also be determined with the horizontal velocity component. The unburned gases exit the burner with zero horizontal velocity and accelerate sideways through the flame front. The corresponding horizontal velocity line can be seen in figure 3.16.

The points are fitted with a 10th order polynomial to obtain the flame front contour. Figure 3.17 shows a sample of the flame front polynomial over the average standard deviation.

This line happens to coincide with the location of the location of the maximal standard deviation. The flame front detection could thus also be determined by looking at only the standard deviation. This overlapping of the flame front and maximum standard deviation is most likely due to the fluctuations of the flame front in time.

The cone angle at a specific location on the flame front is then calculated with the polynomial f(x) as follows:

$$\alpha = \tan^{-1} \frac{f(x+dx) - f(x)}{dx} \tag{3.11}$$

The mean velocity (U_1) from the exit of the burner until the position of the flame front is used as the velocity component. Finally, the laminar burning velocity is calculated with:

$$S_L = U_1 sin\alpha \tag{3.12}$$

3.5. Uncertainties

In this section, the various sources of uncertainties are elaborated upon, for both measurement techniques. The main source of error is due to the fluctuations in the mass flow controllers. OH*-chemiluminescence introduces errors related to the definition of the flame front location. The PIV technique introduces errors due to the seeding and the noise in the PIV measurements.

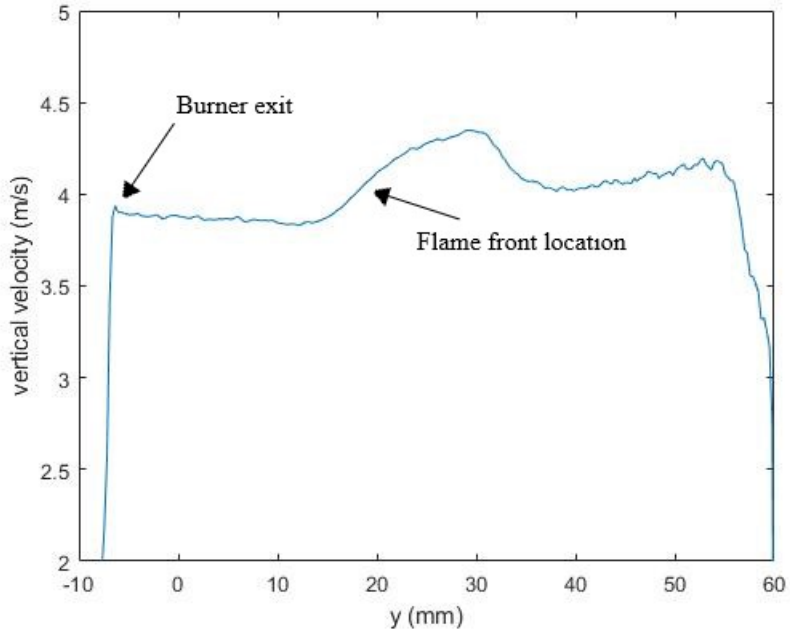

Figure 3.15: Vertical velocity component along evaluated streamline for DNG-hydrogen (50/50) air mixture at 2.81 mm left from the burner centre. (T = 293 K, p = 1 atm)

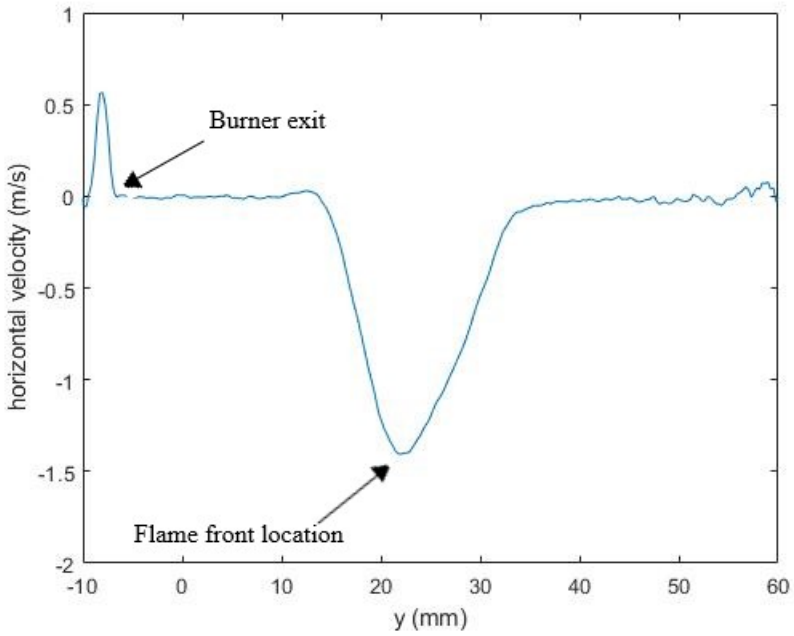

Figure 3.16: Horizontal velocity component along evaluated streamline for DNG-hydrogen (50/50) air mixture at 2.81 mm left from the burner centre. (T = 293 K, p = 1 atm)

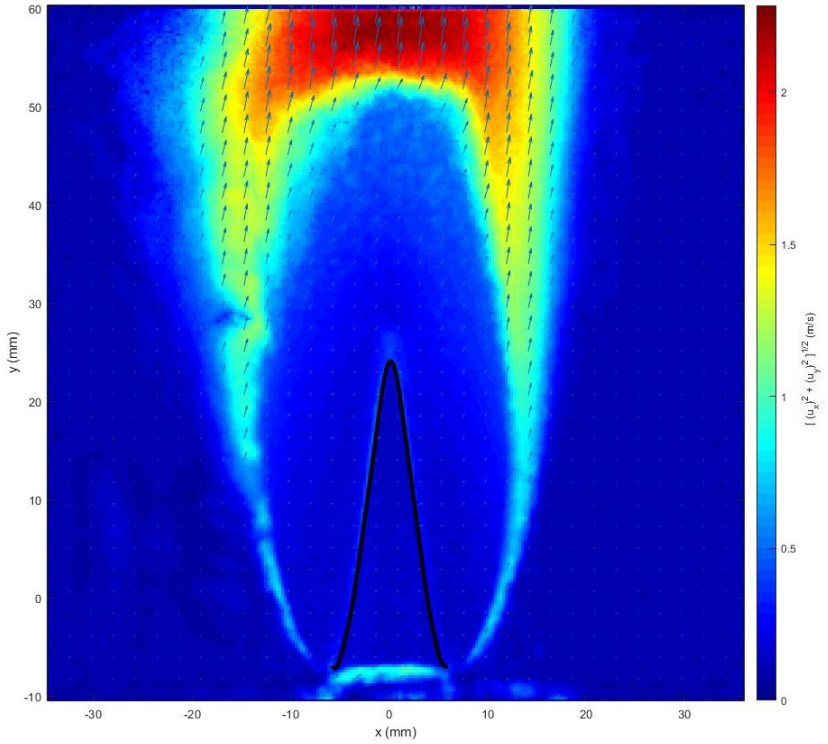

Figure 3.17: Sample of flame front polynomial plotted over the average standard deviation for DNG-hydrogen (50/50) air mixture at 2.81 mm left from the burner centre. (T = 293 K, p = 1 atm)

3.5.1. Mass flow controllers uncertainty

The Bronkhorst are mass flow controllers consist of a thermal mass flow sensor, a precise control valve and a microprocessor-based PID controller with signal and Fieldbus conversion [61]. They are each calibrated for a certain mass flow range. The uncertainties of these controllers are specified as a percentage of full scale (FS) and a percentage of reading (RD). FS is relative to the maximum mass flow the controller is calibrated for. RD is relative to the actual mass flow. The deviation for Rd and Fs are 0.5 and 0.1% respectively, for all 3 mass flow controllers (hydrogen, DNG and air). The accuracy for each controller can thus be noted as follows:

$$\Delta\dot{Q} = 0.005RD + 0.001FS \tag{3.13}$$

Dividing this uncertainty by the inputted mass flow results in the uncertainty expressed in percentage, which will be expressed as u. Higher oscillations are observed when the mass flow controllers operate near the lower operational limit. The individual mass flow controllers are uncorrelated with each other. When assuming a normal distribution for the output of each mass flow controller, one can determine the combined uncertainty in the total volumetric flow rate with the root sum of the squares (RSS) method [66]. The RSS equation is expressed as follows:

$$u(\dot{Q}) = \sqrt{\sum_{i=1}^{n} u(\dot{Q})^2} \tag{3.14}$$

Here, the subscript i represents the numbering in the mixture of n gases. The uncertainty is calculated for both the hydrogen air and DNG-hydrogen air mixtures separately, since their mass flows vary significantly. For simplicity, the mean volumetric flow rate for the different equivalence ratios is used. The pure hydrogen measurements have an uncertainty of $\pm 13\%$ for the air MFC and $\pm 1.75\%$ for the hydrogen MFC. The combined uncertainty for hydrogen air mixtures is $\pm 13.12\%$ for the total volumetric flow rate. Table 3.5 shows the different uncertainties for the mass flow controllers and the total uncertainty for all DNG-hydrogen air mixtures.

Table 3.5: Flow rate uncertainties for different DNG-hydrogen air mixtures

Fuel mixture	air (%)	hydrogen(%)	DNG (%)	total (%)
DNG	5.4	-	3.0	6.2
DNG-h_2 (90/10)	5.4	19.7	3.1	20.7
DNG-h_2 (80/20)	5.4	9.1	3.1	11.0
DNG-h_2 (70/30)	5.4	5.8	3.3	8.6
DNG-h_2 (60/40)	5.3	4.5	3.4	7.7
DNG-h_2 (50/50)	5.3	3.3	3.6	7.2

Fuel mixture	minimum ϕ uncertainty (%)	maximum ϕ uncertainty (%)
DNG	6.1	6.6
DNG-h_2 (90/10)	6.1	6.4
DNG-h_2 (80/20)	6.1	6.3
DNG-h_2 (70/30)	6.0	6.1
DNG-h_2 (60/40)	5.9	6.0
DNG-h_2 (50/50)	5.7	6.0
h_2	13.0	16.9

What is noticeable is the relatively high hydrogen uncertainty for low hydrogen additions. This is because for low hydrogen flow rates, the full scale error has a big influence relatively. The uncertainties in the flow rates translate into equivalence uncertainties, which in turn affect the laminar burning velocity measured. Again, the RSS method is used to determine the minimum and maximum equivalence ratio uncertainty for each fuel composition. Equation (3.15) is used for this computation. Here, the uncertainty introduced on the equivalence ratio for each mass flow controller is calculated. The square root is then taken of the summation of the squared uncertainties.

$$u(\phi) = \sqrt{\sum_{i=1}^{n} u(\phi)^2} \tag{3.15}$$

The uncertainty range represents the change for the proposed equivalence ratio range that will be measured. The equivalence ratio uncertainties translate directly into the change of laminar burning velocity measured, and are accounted for in the error bars in the plots for the OH*-chemiluminescence data.

3.5.2. Unburned gases temperature uncertainty

The laminar burning velocity is strongly dependent on the initial temperature of the reactants. The laboratory in which the experiments are conducted is kept at 293K with a $\pm 2K$ fluctuation. The reactant piping configuration are designed for a length sufficiently long that they exit the burner at the room temperature. The correlation between the laminar burning velocity and the temperature is often expressed as $S_L \sim T_{ug}^n$ [67]. For methane, it is generally accepted that n = 2 and around 1.7 for hydrogen. The uncertainty is $\pm 0.68\%$ for the initial reactant temperature (2K at 293K). This results in a ± 1 $\pm 1.4\%$ uncertainty in the laminar burning velocity for DNG and hydrogen measurements respectively. This uncertainty could contribute to slight discrepancies between different measurement samples if taken at with sufficient time in between. This uncertainty translates into the measured flame-front area and are not present in the error bars for the OH*-chemiluminescence measurements.

3.5.3. specific OH*-chemiluminescence uncertainty

The laminar burning velocity is defined to be relative to the unburned gas mixture. The OH* chemiluminescence methodology defines the flame front area as that of maximum OH* intensity, which is further downstream of the preheating zone. This is schematically illustrated in figure 3.18 which defines the discrepancy between these two locations as the flame thickness.

Since the OH* surface is larger, it will underestimate the laminar burning velocity compared to

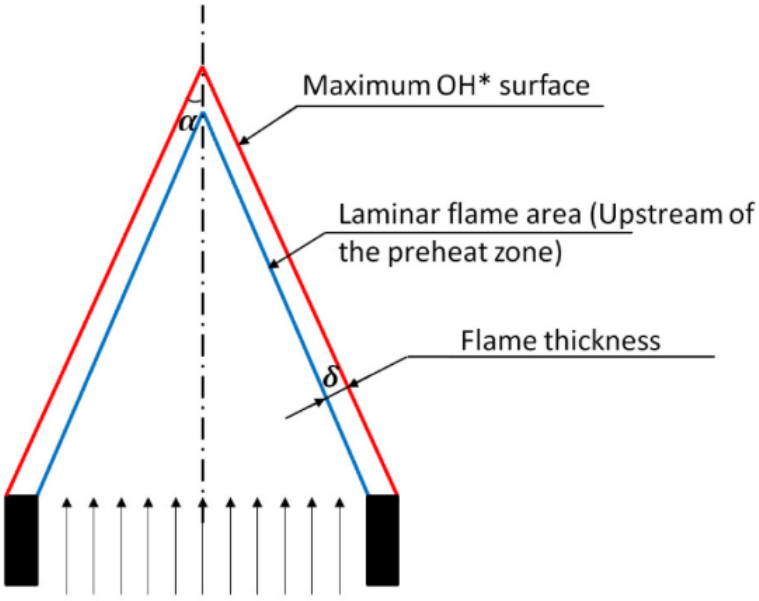

Figure 3.18: Illustration of the OH* surface and laminar flame area [8]

the value taken relative to the upstream of the preheating zone. This discrepancy is correlated with the flame thickness. Andrews and Bradley found that this difference in area is positively correlated with δ/d, in which δ is the flame thickness and d the burner diameter [68]. Increasing the burner diameter should thus decrease the discrepancy between the OH* and unburned flame area. δ cannot be changed for a given fuel composition, as it is dependent on the chemical processes governing the flame propagation. Differences up to 13% in terms of burning velocity are observed when comparing Bunsen flame OH*chemiluminescence measurements obtained with spherical and counterflow flame configurations [6]. This uncertainty is not accounted for in the measurement data error bars.

3.5.4. Specific PIV uncertainties

PIV measurements have numerous error sources. These errors could stem from the system calibration, the optical setup, timing errors as well as other systematic and random errors. The two main factors which determine how accurate the seeding follow the streamlines are due to the thermophoretic effects and the particle lagging effect [69].

Thermophoretic is the phenomenon in which mobile particles in mixture behave differently due to the force of a temperature gradient [70]. For the seeding particles, this phenomenon results in a net force in the opposite direction to the temperature gradient in the flow. The temperature gradient is the highest in the flame front. This can result in a significant lag in the particle velocity compared to the actual velocity [70]. The temperature gradient is however minimal upstream of the preheating zone. Since the velocity vector needed for the measurement of the laminar burning velocity is the mean from the burner exit to the beginning of the flame front, this should have a minimal impact on the obtained burning velocity measurements.

The other main factor for the accuracy related to the particle velocity is the particle lagging effect. This is the source of error because of gravitational forces due to the densities of the gaseous mixture and particle seedings not matching. This is quantified by the Stokes' equation given in (3.16)

$$Stk = Re\frac{\rho_p d_p^2}{\rho_{ug} L^2} \tag{3.16}$$

Where Re is the Reynolds number, ρ_p and ρ_f are the particle and unburned gas mixture densities respectively, d_p^2 is the particle diameter and L the characteristic PIV window dimension. A Stokes' number (Stk) significantly lower than unity indicates that the particle lagging effect is not significant. the

solid particle chemical compound Al_2O_3, has a density of 3920 $\frac{kg}{m^3}$ with a diameter of 1μm. The maximum Reynolds number for the PIV measurements is 1800. With a minimum density of the unburned gas mixture of 0.93 $\frac{kg}{m^3}$ and an L of 0.07 m, the Stk is as follows:

$$Stk = 1800\frac{3290 \cdot (1 \cdot 10^{-5})^2}{0.93 \cdot 0.07^2} = 0.13 \tag{3.17}$$

Since 0.13 « 1, the particle lagging effect is not significant and tracing accuracies should be below 1% [71].

4

Results and discussion

The laminar burning velocities measurements performed with the Bunsen burner method, in combination with OH*-chemiluminescence and PIV, are presented and discussed in this chapter. The results are plotted against computational results with the GRI 3.0 kinetic mechanism. The first part of this chapter presents and discusses the validation procedure performed with pure hydrogen measurements. In the second part, the Bunsen burner in combination with OH*-chemiluminescence measurements are presented and discussed. Finally, the results obtained with PIV are presented, compared and discussed with the numerical and OH*-chemiluminescence results.

4.1. Validation with pure hydrogen

Preliminary experiments are conducted with hydrogen air mixtures, in order to validate the OH* chemiluminescence optical diagnostics and the post-processing technique of the images to obtain the laminar burning velocity. These are performed for the equivalence ratio range 0.7-2.1 in 0.1 step-sizes. The measurements are performed at ambient conditions (T = 293K, p = 1 atm). The Reynolds number is set at 1750 in order to obtain laminar flow, which translates to an unburned gas velocity of 9 $\frac{m}{s}$. The results are presented in figure 4.1 together with the numerical results obtained with the GRI 3.0 kinetic mechanism. The error bars represent the 95% confidence interval. Table 4.1 presents the experimental results together with the simulation with there deviation.

Table 4.1: Laminar burning velocity comparison between experimental results and simulated results using GRI-Mech 3.0 for hydrogen air mixture. Difference is increase w.r.t Experimental result (T = 293 K, p = 1 atm)

Equivalence ratio	Experimental result (cm/s)	GRI-Mech 3.0 (cm/s)	Difference (%)
0.7	109	119	9.17
0.8	133	159	19.5
0.9	175	195	11.4
1.0	191	225	17.8
1.1	230	250	8.70
1.2	241	270	12.0
1.3	253	284	12.3
1.4	266	294	10.5
1.5	280	300	7.14
1.6	289	303	4.84
1.7	285	303	6.32
1.8	282	301	6.74
1.9	281	297	5.69
2.0	277	292	5.42
2.1	274	286	4.38

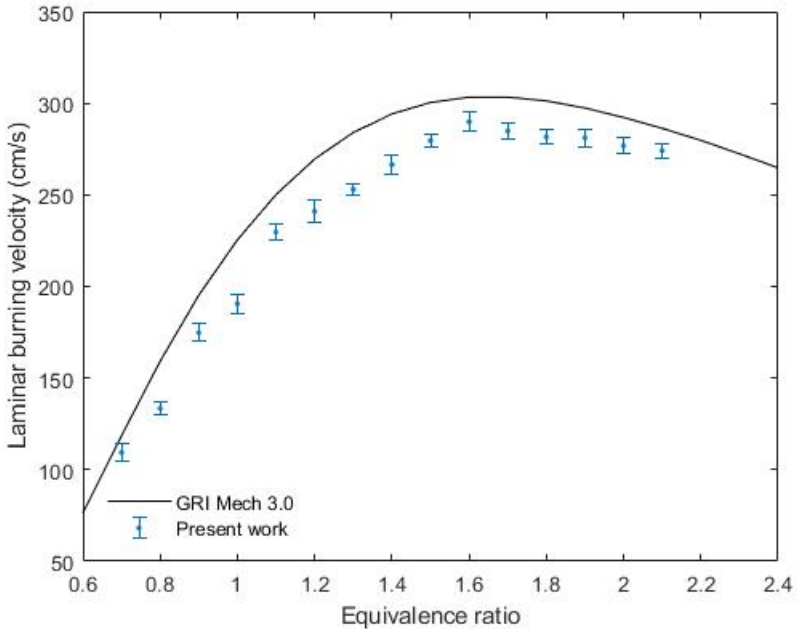

Figure 4.1: Laminar burning velocity comparison between experimental results and simulated results using GRI-Mech 3.0 for hydrogen air mixture. Error bars represent 95% confidence interval (T = 293 K, p = 1 atm)

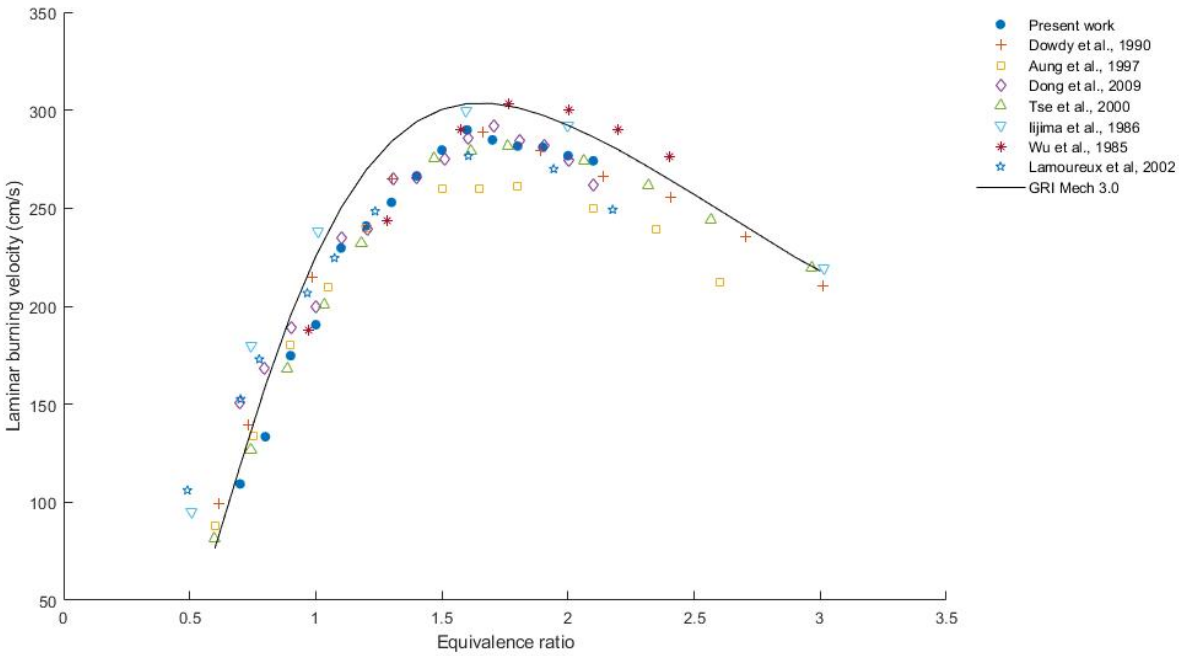

Figure 4.2: Laminar burning velocity versus equivalence ratio for hydrogen air mixture obtained from literature and present work (T = 291 - 298 K, p = 1 atm)

Figure 4.2 presents the experimental results plotted with the measurements found in the literature. Bowdy et al. (1990) [72], Aung et al. (1997) [73], Tse et al. (2000) [74], Iijima et al. (1986) [75] and Lamoureux et al. (2002) [76] all use the spherical flame method. Dong et al. (2009) [77] and Wu et al. (1985) [78] both use the Bunsen burner method with the mass conservation and semi-cone angle method respectively.

The maximum laminar burning velocity from the experimental result is 289 $\pm$ 5 cm/s. The 95% confidence interval is in the range $\pm$ 3-6 cm for the experiments. Figure 4.1 show that the GRI-Mech 3.0 kinetic mechanism predictions are a bit higher than the experimental results. This trend is mainly because the experimental results are not adiabatic due to the heat losses and the stretch effects. The numerical results are for adiabatic unstretched flames. A difference up to 17.8% is observed for equivalence 1. The difference tends to decrease with increasing equivalence ratio and is around 6% for the rich region. This difference could due to the tip opening that is observed for equivalence ratio below 1.2, and the data processing that is applied to open tip flames. This is elaborated upon later in this section.

Figure 4.2 shows that the overall agreement between the different experimental results is generally good. The experimental results to the lean side of the maximum laminar burning velocity, achieved for an equivalence ratio 1.6, are in good agreement with each other with an exception for Iijima et al. [75], which tends to overestimate. The scatter is larger to the rich side of 1.6, with Aung et al. [73] underestimating and Wu et al. [78] overestimating compared to the present experimental points. The difference can be attributed to the different measurement techniques and methodologies used in these studies. Nevertheless, the current experimental work are in good agreement with the literature. The optical diagnostics and post-processing technique for the OH*-chemiluminescence method can thus be used with confidence in their accuracy.

4.1.1. Tip opening

An interesting phenomenon that is observed is the tip opening for the leaner hydrogen air flames. Tip opening in laminar premixed Bunsen flames is directly related to the stretch rate and the preferential diffusion [79]. The concave curvature at the tip of the Bunsen burner results in a focusing effect of the heat towards the fresh reactants. In other words, a larger segment of the flame heats the fresh reactant. The opposite effect however occurs for the fresh reactant towards the flame, since fresh reactants defocus to a larger segment of the flame. The burning intensity of the curved segment of the flame is therefore directly related to the Lewis number, Le. This number is defined as the ratio between the mixture thermal diffusivity to the mass diffusivity of the deficient reactant.

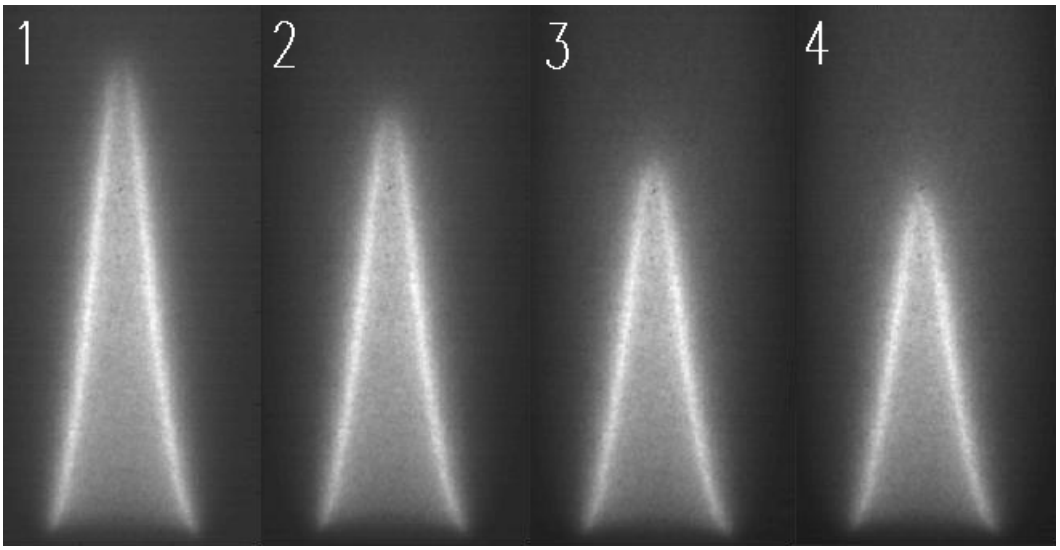

Figure 4.3: OH*-chemiluminescence images of hydrogen air flames with (1) = 1.0 ϕ, (2) = 1.1 ϕ, (3) = 1.2 ϕ and (4) = 1.3 ϕ (T = 293 K and p = 1 atm)

The OH*-chemiluminescence images in figure 4.3 show that the tip opening occurs between equivalence ratio 1.1-1.2. This decrease in burning intensity is characterized by a Lewis number lower than unity, implying that the mass diffusivity exceeds the thermal diffusivity. Previous studies have observed tip opening for rich propane air and butane air flames [79] as well as hydrogen air flames for an equivalence ratio between 1-1.15 [80]. All these experiments have shown an agreement between a decrease of the burning intensity at the tip and eventual extinction, and a Lewis number less than unity (Le<1).

A Lewis number more than unity showed an increase in the burning intensity at the curved segment of the flame.

The flame tip opening results in complications in the post-processing of the OH*-chemiluminescence. Logically, one would expect an incomplete combustion at the flame tip due to fuel leakage. Kozlovsky et al. [81] conducted a numerical study about Bunsen flames characterized by tip opening due to a Lewis number less than unity. They found that even though the reaction rate drops near the tip. the flame survives and manages to consume fully consume the supplied fuel. There is thus no fuel leakage through the flame. Therefore in the current experiments, the open tip images are analyzed from the truncated flame front area and closed off for the open tips.

4.2. Bunsen burner with OH*-chemiluminescence

The results of the laminar burning velocity measurements obtained with OH*-chemiluminescence are presented in this section. The measured fuel compositions are DNG with hydrogen addition from 0 to 50% volumetric addition, in 10% increments. These are performed for the equivalence ratio range 0.8-1.6 in 0.1 step-sizes. The measurements are performed at ambient conditions (T = 293K, p = 1 atm). The Reynolds number is set at 1600 in order to obtain laminar flow. The experimental results are plotted against numerical simulations obtained with the GRI-Mech 3.0 kinetic mechanism. The literature does not contain DNG or DNG-hydrogen laminar burning velocity measurements, thus no comparison could be made with existing data.

DNG-air measurements are presented in figure 4.4 together with the GRI-Mech 3.0 results. The maximum laminar burning velocity of 35.3 $\pm$ 0.2 cm/s is measured at equivalence ratio 1.1. The accuracy for the measurements according to the 95% confidence interval are within the range $\pm$ 0.1 - 0.3 cm/s. The exact values are given in 4.2. The equivalence ratio range is limited at 0.95 due to blow-off. The experimental results are in good agreement with GRI-Mech 3.0 for equivalence ratio 1.2 and lower, and 1.6. Equivalence 1.3-1.5 shows a significant deviation of 20-30% compared with numerical results.

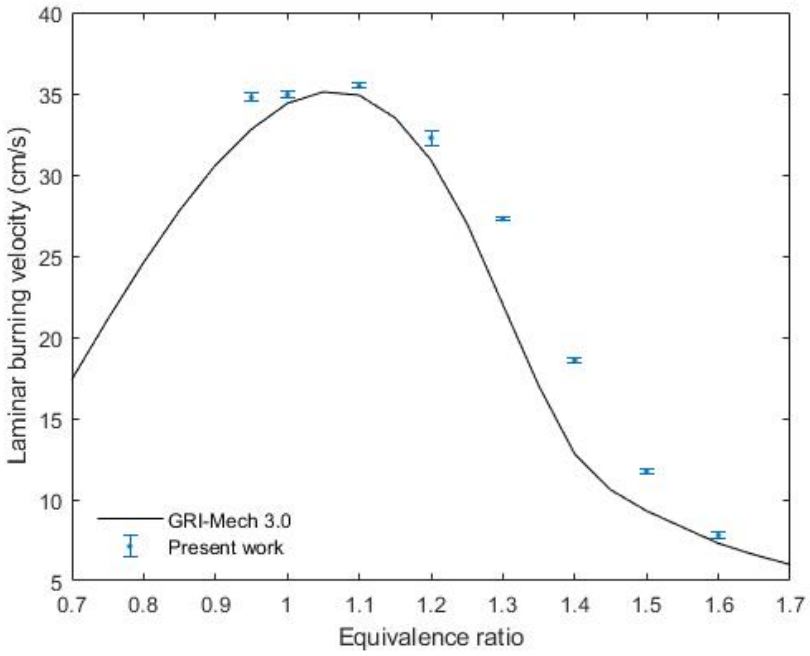

Figure 4.4: Laminar burning velocity comparison between experimental results and simulated results using GRI-Mech 3.0 for DNG air mixture. Error bars represent 95% confidence interval (T = 293 K, p = 1 atm)

This discrepancy could be attributed due to the inability of GRI-Mech 3.0 to capture the laminar

Table 4.2: Laminar burning velocity comparison between experimental results and simulated results using GRI-Mech 3.0 for DNG air mixture. Difference is increase w.r.t Experimental result (T = 293 K, p = 1 atm)

Equivalence ratio	Experimental result (cm/s)	GRI-Mech 3.0 (cm/s)	Difference (%)
0.95	34.8	32.8	5.75
1.0	34.9	34.4	1.43
1.1	35.5	34.9	1.69
1.2	32.3	30.9	4.04
1.3	27.9	22.0	21.2
1.4	18.6	12.8	31.2
1.5	11.7	9.3	20.5
1.6	7.81	7.3	6.53

burning velocity of the DNG mixture containing methane with other higher order hydrocarbons and a larger volumetric fraction of inert gases (14% N_2), in the rich region. The GRI-Mech 3.0 simulation is performed with the DNG composition as presented in table 4.3 [15]. However, the natural gas from the Dutch gas network is sometimes supplied with imported gas consisting of a different composition [82]. This could have resulted in a different gas composition used in the experiments. The imported gas is added such that the calorific value is equal. The relation between the calorific value and the laminar burning velocity is only linear in the lean region [83]. This could explain why the discrepancy is the largest in the rich region.

Table 4.3: Volumetric fractions Dutch natural Gas

Species	Volumetric fraction [%]
CH_4	81.3
C_2H_6	2.9
C_3H_8	0.4
C_4H_{10}	0.2
N_2	14.3
CO_2	0.9

DNG-hydrogen air measurements for 10, 20, 30, 40 and 50% volumetric hydrogen addition are presented in figure 4.5, 4.6, 4.7, 4.8 and 4.9 respectively. The exact values are given in table 4.4, 4.5, 4.6, 4.7 and 4.8 respectively. The measurements are limited to equivalence ratio 1 for the 10% hydrogen addition. This is due to the lower limit of the hydrogen mass flow controller. For 20% hydrogen addition, the limit due to blow-off is at equivalence ratio 0.9. For 30% hydrogen addition, this is at 0.85 equivalence ratio. Both the 40% and 50% hydrogen addition cases were able to stabilize a flame at the lower limit of 0.8 equivalence ratio. This increase in the blow-off stability criteria with increasing hydrogen addition is due to the increase of laminar burning velocity. Figure 4.10 presents all DNG-hydrogen air mixture measurements. The maximum laminar burning velocity increases from 35.3 $\pm$ 0.2 cm/s (0% H_2) to 37.2 $\pm$ 0.3 cm/s (10% H_2), 41.4 $\pm$ 0.2 cm/s (20% H_2), 46.3 $\pm$ 0.3 cm/s (30% H_2), 52.9 $\pm$ 0.3 cm/s (40% H_2) and 62.2 $\pm$ 0.4 cm/s (50% H_2). All maximum burning velocities are achieved for equivalence ratio 1.1.

The same discrepancy trend when comparing to GRI-Mech 3.0 predictions is obtained for all hydrogen additions. The measurements are in good agreement in the lean region for all fuel compositions. The maximum discrepancy is, just as for the 100% DNG case, obtained for the equivalence ratio range 1.3-1.5, which is consistently 20-35% for all cases. This could again be attributed with the same reasoning as given for 100% DNG. The strong agreement in the lean region for all cases gives more weight to the argument that the natural gas composition could be different since the same calorific value has a linear correlation with the laminar burning velocity in the lean region.

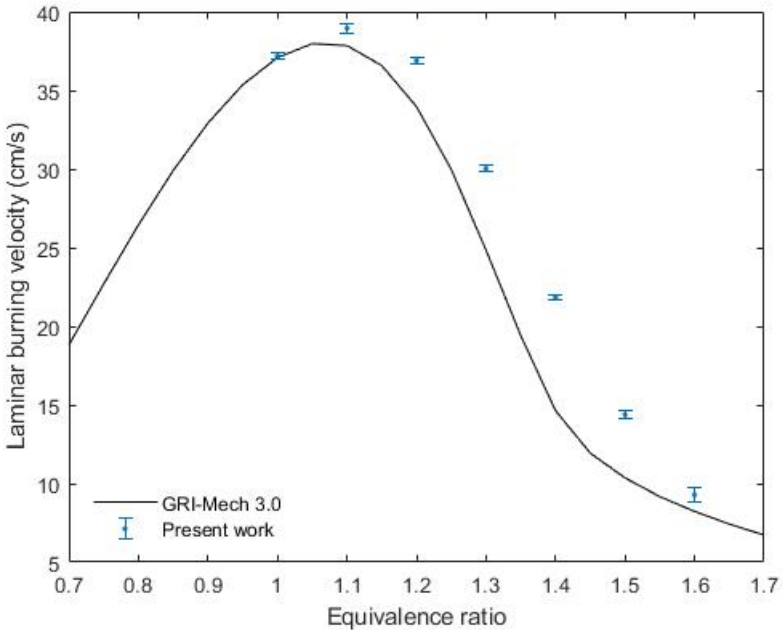

Figure 4.5: Laminar burning velocity comparison between experimental results and simulated results using GRI-Mech 3.0 for DNG-hydrogen (90/10) air mixture. Error bars represent 95% confidence interval (T = 293 K, p = 1 atm)

Table 4.4: Laminar burning velocity comparison between experimental results and simulated results using GRI-Mech 3.0 for DNG-hydrogen (90/10) air mixture. Difference is increase w.r.t Experimental result (T = 293 K, p = 1 atm)

Equivalence ratio	Expertimental result (cm/s)	GRI-Mech 3.0 (cm/s)	Difference (%)
1.0	37.2	37.1	0.27
1.1	39.0	37.9	2.82
1.2	36.9	34.0	7.86
1.3	30.0	24.8	17.3
1.4	21.8	14.6	33.0
1.5	14.4	10.4	27.8
1.6	9.29	8.233	11.4

Table 4.5: Laminar burning velocity comparison between experimental results and simulated results using GRI-Mech 3.0 for DNG-hydrogen (80/20) air mixture. Difference is increase w.r.t Experimental result (T = 293 K, p = 1 atm)

Equivalence ratio	Expertimental result (cm/s)	GRI-Mech 3.0 (cm/s)	Difference (%)
0.9	36.7	35.8	2.45
1.0	41.4	40.4	2.24
1.1	42.0	41.5	1.19
1.2	40.4	37.7	6.68
1.3	33.9	28.4	16.2
1.4	25.2	17.2	31.5
1.5	17.4	11.7	32.8
1.6	11.2	9.31	16.9

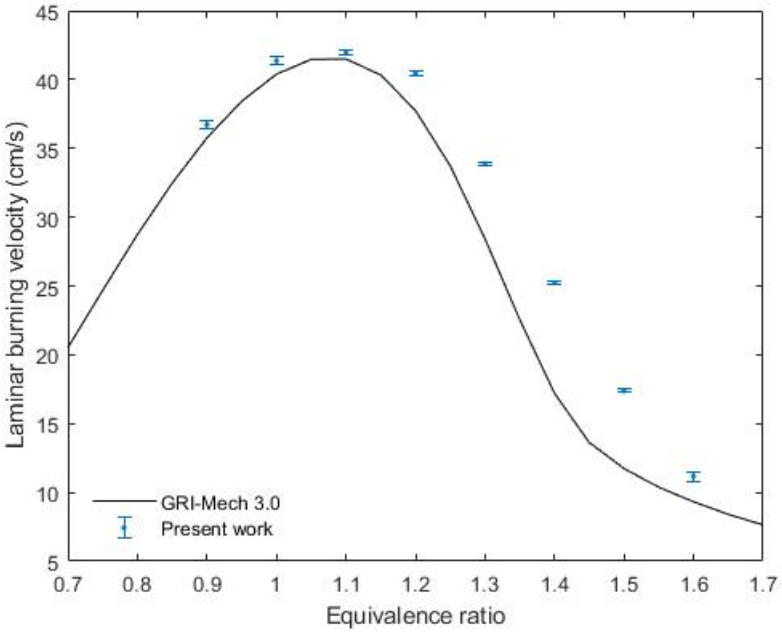

Figure 4.6: Laminar burning velocity comparison between experimental results and simulated results using GRI-Mech 3.0 for DNG-hydrogen (80/20) air mixture. Error bars represent 95% confidence interval (T = 293 K, p = 1 atm)

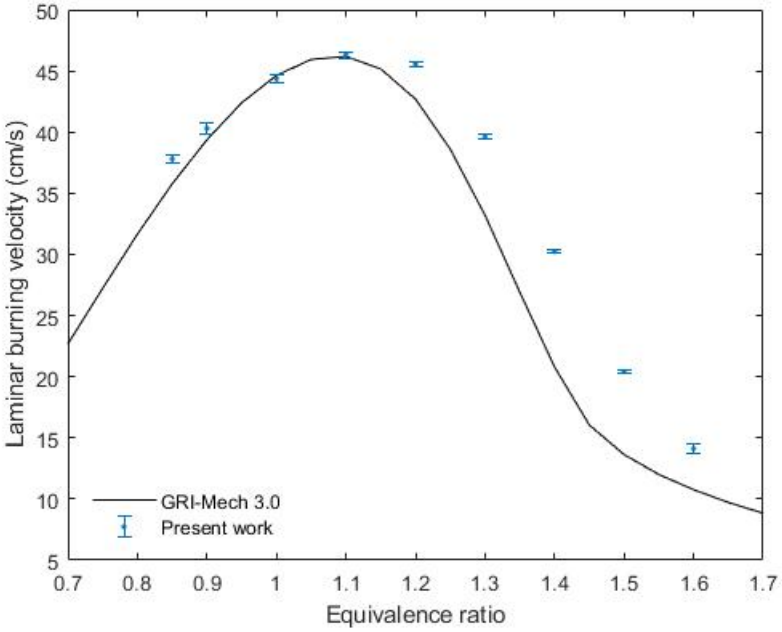

Figure 4.7: Laminar burning velocity comparison between experimental results and simulated results using GRI-Mech 3.0 for DNG-hydrogen (70/30) air mixture. Error bars represent 95% confidence interval (T = 293 K, p = 1 atm)

Table 4.6: Laminar burning velocity comparison between experimental results and simulated results using GRI-Mech 3.0 for DNG-hydrogen (70/30) air mixture. Difference is increase w.r.t Experimental result (T = 293 K, p = 1 atm)

Equivalence ratio	Expertimental result (cm/s)	GRI-Mech 3.0 (cm/s)	Difference (%)
0.85	37.8	35.8	5.29
0.9	40.3	39.4	2.23
1.0	44.4	44.6	0.45
1.1	46.3	46.2	0.22
1.2	45.6	42.7	6.36
1.3	39.6	33.2	16.2
1.4	30.2	20.8	31.1
1.5	20.4	13.6	33.3
1.6	14.1	10.8	23.4

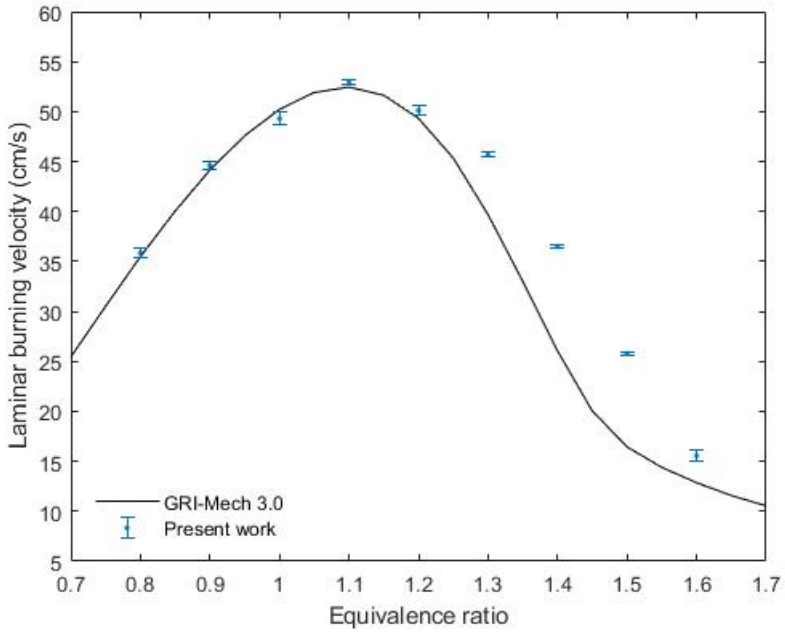

Figure 4.8: Laminar burning velocity comparison between experimental results and simulated results using GRI-Mech 3.0 for DNG-hydrogen (60/40) air mixture. Error bars represent 95% confidence interval (T = 293 K, p = 1 atm)

Table 4.7: Laminar burning velocity comparison between experimental results and simulated results using GRI-Mech 3.0 for DNG-hydrogen (60/40) air mixture. Difference is increase w.r.t Experimental result (T = 293 K, p = 1 atm)

Equivalence ratio	Expertimental result (cm/s)	GRI-Mech 3.0 (cm/s)	Difference (%)
0.8	35.8	35.5	0.84
0.9	44.6	44.2	0.90
1.0	49.3	50.2	1.83
1.1	52.9	52.5	0.76
1.2	50.1	49.3	1.60
1.3	45.7	39.7	13.1
1.4	36.5	26.0	28.8
1.5	25.8	16.5	36.0
1.6	15.6	12.9	17.3

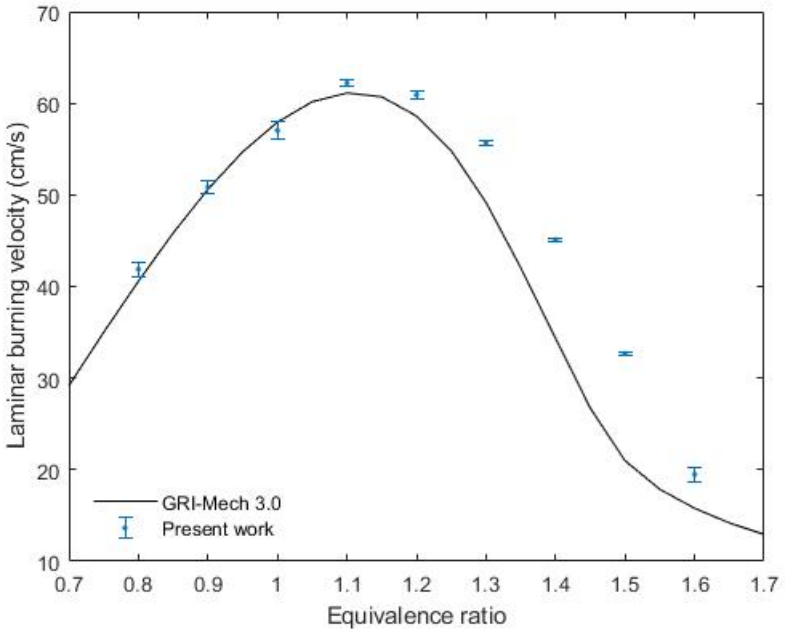

Figure 4.9: Laminar burning velocity comparison between experimental results and simulated results using GRI-Mech 3.0 for DNG-hydrogen (50/50) air mixture. Error bars represent 95% confidence interval (T = 293 K, p = 1 atm)

Table 4.8: Laminar burning velocity comparison between experimental results and simulated results using GRI-Mech 3.0 for DNG-hydrogen (50/50) air mixture. Difference is increase w.r.t Experimental result (T = 293 K, p = 1 atm)

Equivalence ratio	Expertimental result (cm/s)	GRI-Mech 3.0 (cm/s)	Difference (%)
0.8	41.9	40.6	3.10
0.9	50.8	50.6	0.39
1.0	57.0	57.9	1.58
1.1	62.2	61.1	1.77
1.2	60.9	58.6	3.78
1.3	55.7	49.2	11.7
1.4	45.1	34.3	23.9
1.5	32.7	21.0	35.8
1.6	19.5	15.8	18.9

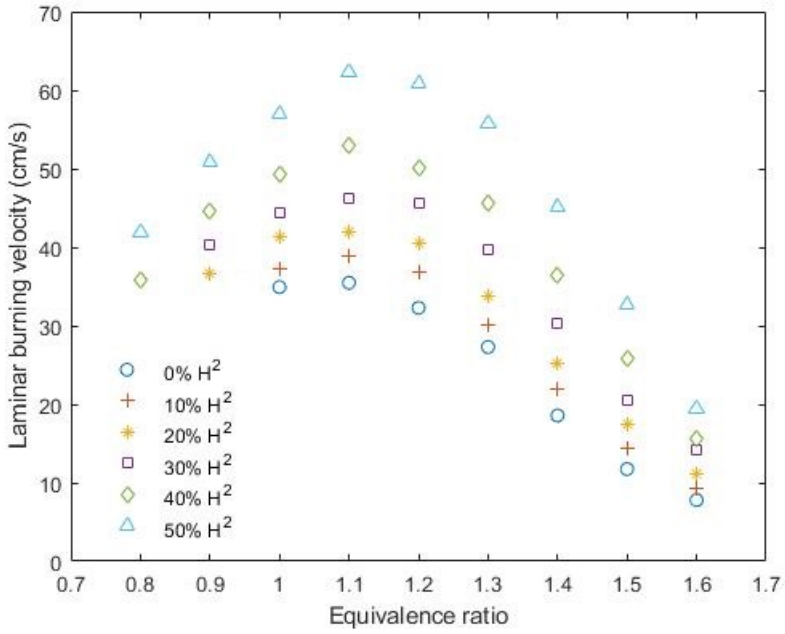

Figure 4.10: Laminar burning velocity versus equivalence ratio from experimental results, for DNG-hydrogen 10-50% air mixture, in 10% increments (T = 293 K, p = 1 atm)

4.3. Bunsen burner with PIV

The results obtained with PIV are presented in this section. The 12 measurement points are presented in table 4.9.

Table 4.9: Measurement points for PIV

Fuel mixture (vol. %)	equivalence ratios	Reynolds number	Unburned gas velocity (m/s)
DNG	1.0 and 1.4	1100	1.21
DNG	1.0 and 1.4	1600	1.81
DNG-hydrogen (80/20)	1.0 and 1.4	1600	1.85
DNG-hydrogen (80/20)	1.0 and 1.4	1800	1.85
DNG-hydrogen (50/50)	1.0 and 1.4	1600	1.94
DNG-hydrogen (50/50)	1.0 and 1.4	1800	2.21

Three different fuel compositions are measured for two different equivalence ratios. Each measurement point is performed for two different unburned gas velocities. The PIV results are compared with the results obtained from OH*-chemiluminescence and GRI-Mech 3.0. For each measurement point, the velocity field is presented with the contour of the flame front. The evolution of the laminar burning velocity over the flame front is also presented. The tip of the Bunsen flame undergoes significant fluctuations during the 4 second measurement time, due to re-circulation of the ambient air. The curvature of the flame tip could therefore not be captured accurately enough and thus the laminar burning velocity cannot be calculated in this region. The evolution of the laminar burning velocity at the tip region is therefore not presented.

4.3.1. DNG air mixture

DNG air mixtures are measured for both equivalence ratio 1.0 and 1.4, at 1100 and 1600 Reynolds number. Figure 4.11 shows the velocity field for equivalence ratio 1.0 and 1100 Re, with figure 4.12 the corresponding laminar burning velocity plot over the flame front. Figure 4.13 shows the velocity field for equivalence ratio 1.4 and 1100 Re, with figure 4.14 the corresponding laminar burning velocity plot over the flame front. Figure 4.15 and 4.16 show the velocity field and laminar burning velocity over the flame front plot for equivalence ratio 1.4 and 1100 respectively. The velocity field and laminar

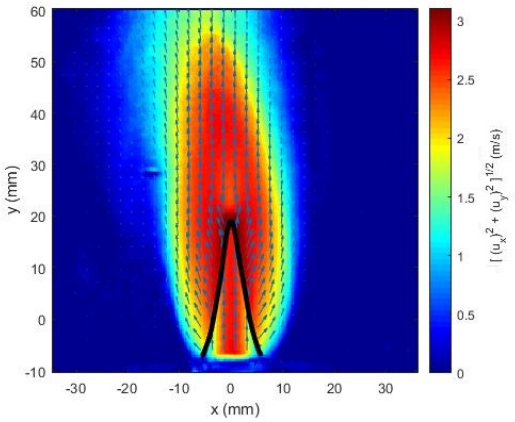

Figure 4.11: Velocity field for DNG air mixture for ϕ = 1.0 and 1100 Re (T = 293K, p = 1 atm)

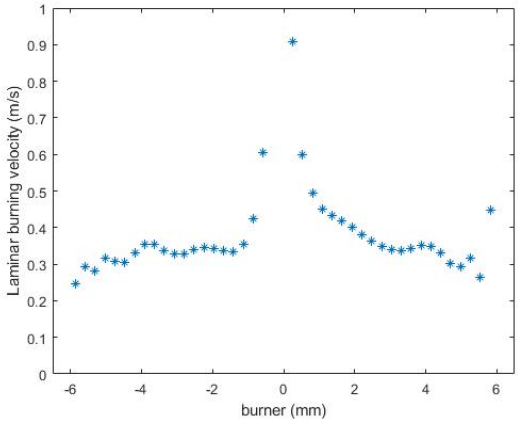

Figure 4.12: Laminar burning velocity versus flame front location for DNG air mixture for ϕ = 1.0 and 1100 Re (T = 293K, p = 1 atm)

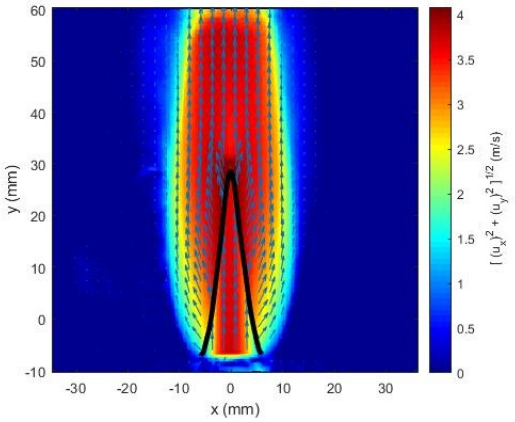

Figure 4.13: Velocity field for DNG air mixture for ϕ = 1.0 and 1600 Re (T = 293K, p = 1 atm)

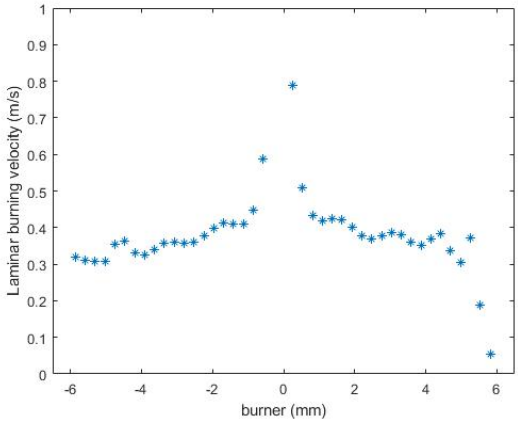

Figure 4.14: Laminar burning velocity versus flame front location for DNG air mixture for ϕ = 1.0 and 1600 Re (T = 293K, p = 1 atm)

burning velocity plot for Equivalence ratio 1.4 and 1600 Reynolds number are shown in figure 4.17 and 4.18 respectively.

The x-axis represents the burner, with 0 mm being the centre. All laminar burning velocity plots show an increase of the burning velocity towards the tip, due to an increase in the curvature. The laminar burning velocities calculated near the burner rim, thus the outer points, can be discarded due to noise. The laminar burning velocity cannot be extracted at these locations because of the heat losses and resolution of the velocity field. The cone-angle and mean velocity vector can therefore not be extracted accurately enough. Some fluctuations are present in the burning velocity measurements in the base of the flame. This is more prominent in the 1.0 equivalence ratio plots. Both sides of the flame also are not fully symmetrical. This is due to the disturbance of the flow field by both the seeding particles as well as the mass flow controllers. The seeding devices used for these measurements were not able to sufficiently seed the gas mixture in a continuous manner. To circumvent this problem, the seeding devices were shaken at the start of each measurement. This resulted in an uneven flow of seeding. At the start of each measurement, the seeding density was relatively high and then slowly decreased. This seeding pulse resulted in significant fluctuations on the Bunsen flame, which explains the unsymmetrical nature of the laminar burning velocity measurements, as well as the slight fluctuations over the base. The 1.0 equivalence ratio case shows larger fluctuations because the laminar burning velocity is higher. This results in a larger temperature gradient, and thus larger seeding inaccuracies

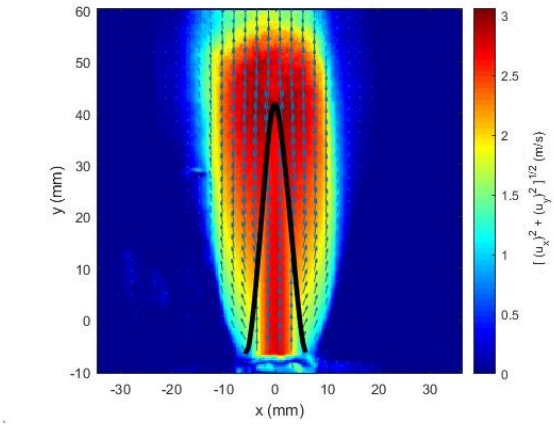

Figure 4.15: Velocity field for DNG air mixture for ϕ = 1.4 and 1100 Re (T = 293K, p = 1 atm)

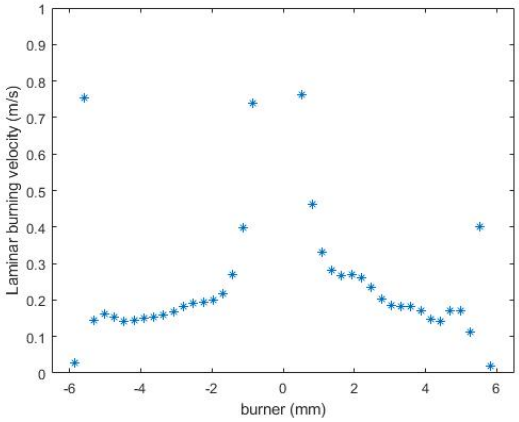

Figure 4.16: Laminar burning velocity versus flame front location for DNG air mixture for ϕ = 1.4 and 1100 Re (T = 293K, p = 1 atm)

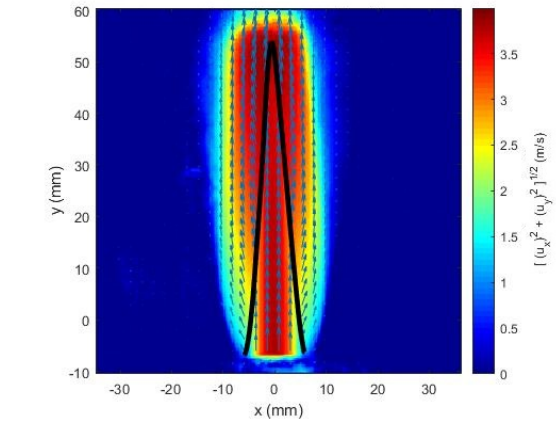

Figure 4.17: Velocity field for DNG air mixture for ϕ = 1.4 and 1600 Re (T = 293K, p = 1 atm)

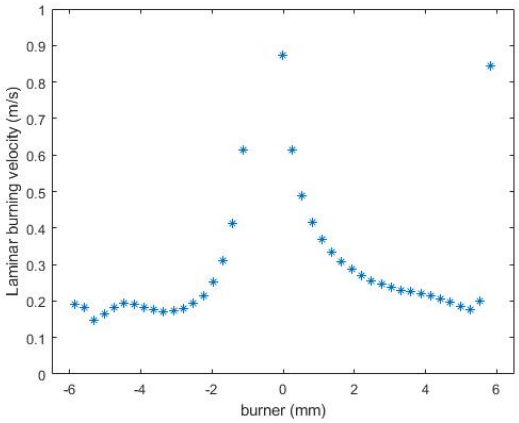

Figure 4.18: Laminar burning velocity versus flame front location for DNG air mixture for ϕ = 1.4 and 1600 Re (T = 293K, p = 1 atm)

Table 4.10: Laminar burning velocities obtained from PIV at base of flame for DNG air mixture at ϕ = 1.0 and 1100 and 1600 Re, compared with OH* and GRI-Mech 3.0 results (T = 293K, p = 1 atm)

Laminar burning velocity (cm/s)				**Difference wrt 1100 Re (%)**		
1100 Re	1600 Re	OH*	GRI-Mech 3.0	1600 Re	OH*	GRI-Mech 3.0
34.7	35.2	35.0	34.4	1.44	0.86	-0.86

Table 4.11: Laminar burning velocities obtained from PIV at base of flame for DNG air mixture at ϕ = 1.4 and 1100 and 1600 Re, compared with OH* and GRI-Mech 3.0 results (T = 293K, p = 1 atm)

Laminar burning velocity (cm/s)				**Difference wrt 1100 Re (%)**		
1100 Re	1600 Re	OH*	GRI-Mech 3.0	1600 Re	OH*	GRI-Mech 3.0
16.9	18.2	18.6	12.8	7.69	10.06	24.26

due to thermophoretic effects.

The laminar burning velocity is extracted from the base of the flame. The assumption is made that this region measured the unstretched laminar burning velocity since no curvature is present. 4 mm from the burner centre is chosen for all measurements for consistency. The average for both halves of the flame is taken. Table 4.10 presents the laminar burning velocity obtained with PIV for equivalence ratio 1.0 for both Reynolds numbers, and compared with OH* and GRI-Mech 3.0. Both Reynolds numbers calculations are in good agreement which each other. They are also in good agreement with both OH* and GRI-Mech 3.0. Table 4.11 presents the PIV results for equivalence ratio 1.4 and Reynolds number 1100 and 1600. Both Reynolds numbers are in good agreement with each other, with only a 0.82% difference. The discrepancy with OH*-chemiluminescence is also only 2.86%. However, it has a 24.26% discrepancy with the GRI-Mech 3.0, as this tends to underestimate the burning velocity for equivalence 1.4, in the same trend as when compared to OH*-chemiluminescence.

4.3.2. DNG-hydrogen (80/20) air mixture

DNG with 20% volumetric hydrogen addition air mixtures are measured for both equivalence ratio 1.0 and 1.4, at 1600 and 1800 Reynolds number. Figure4.19 shows the velocity field for equivalence ratio 1.0 and 1100 Re, with figure 4.20 the corresponding laminar burning velocity plot over the flame front. Figure 4.21 shows the velocity field for equivalence ratio 1.4 and 1100 Re, with figure 4.22 the corresponding laminar burning velocity plot over the flame front. Figure 4.23 and 4.24 show the velocity field and laminar burning velocity over the flame front plot for equivalence ratio 1.4 and 1100 respectively. The velocity field and laminar burning velocity plot for Equivalence ratio 1.4 and 1600 Reynolds number are shown in figure4.25 and 4.26 respectively.

The same fluctuations as for 100% DNG and asymmetry in the laminar burning velocity is observed for the 20% hydrogen addition measurements. Again, the 1.0 equivalence ratio measurements tend to have a larger fluctuation. Table 4.12 presents the laminar burning velocity obtained with PIV for 20% hydrogen addition mixtures for equivalence ratio 1.0 for both Reynolds numbers, and compared with OH* and GRI-Mech 3.0. Both Reynolds numbers calculations are in good agreement which each other. They are also in good agreement with both OH* and GRI-Mech 3.0. Table 4.11 presents the PIV results for equivalence ratio 1.4 and Reynolds number 1100 and 1600. Both Reynolds numbers are also in good agreement with each other and with the OH*-chemiluminescence measurement. However also in this case, as with the previous measurements, a large discrepancy of 24.26% is found compared to the GRI-Mech 3.0 for equivalence ratio 1.4. GRI-Mech 3.0 tends to underestimate the laminar burning velocity compared to the PIV and OH*-chemiluminescence results.

Table 4.12: Laminar burning velocities obtained from PIV at base of flame for DNG-hydrogen (80/20) air mixture at ϕ = 1.0 and 1600 and 1800 Re, compared with OH* and GRI-Mech 3.0 results (T = 293K, p = 1 atm)

Laminar burning velocity (cm/s)				**Difference wrt 1600 Re (%)**		
1600 Re	1800 Re	OH*	GRI-Mech 3.0	1800 Re	OH*	GRI-Mech 3.0
40.3	40.0	41.4	40.4	0.74	3.47	0.25

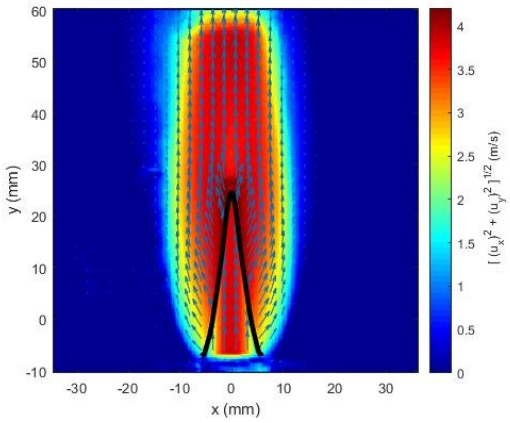

Figure 4.19: Velocity field for DNG/hydrogen (80/20) air mixture for ϕ = 1.0 and 1600 Re (T = 293K, p = 1 atm)

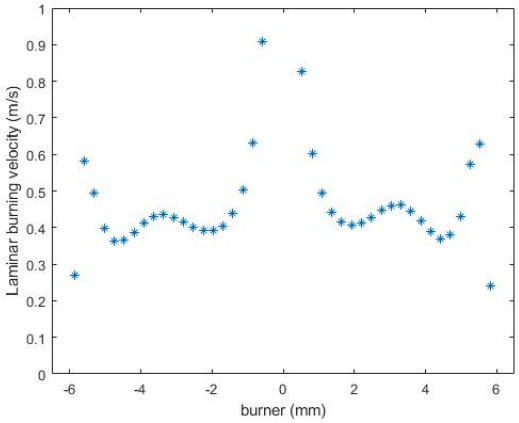

Figure 4.20: Laminar burning velocity versus flame front location for DNG/hydrogen (80/20) air mixture for ϕ = 1.0 and 1600 Re (T = 293K, p = 1 atm)

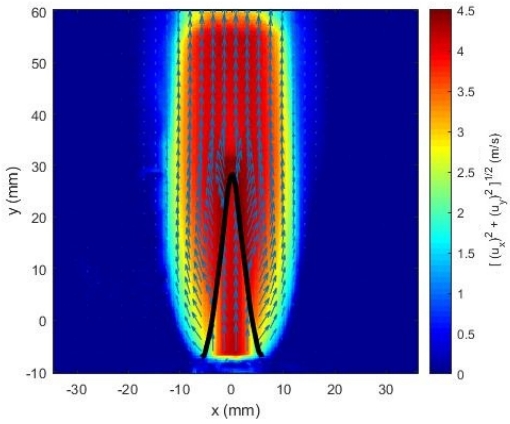

Figure 4.21: Velocity field for DNG/hydrogen (80/20) air mixture for ϕ = 1.0 and 1800 Re (T = 293K, p = 1 atm)

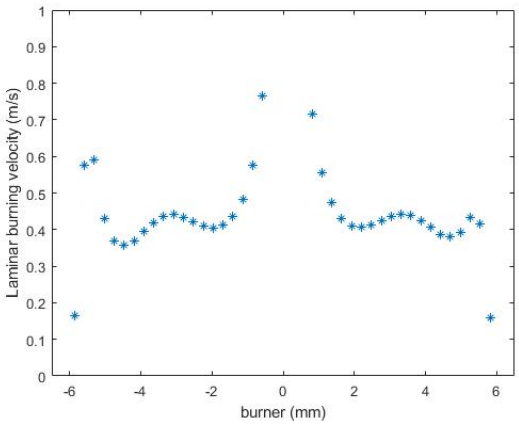

Figure 4.22: Laminar burning velocity versus flame front location for DNG/hydrogen (80/20) air mixture for ϕ = 1.0 and 1800 Re (T = 293K, p = 1 atm)

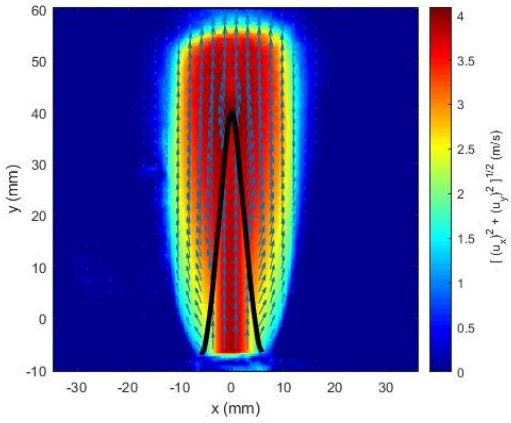

Figure 4.23: Velocity field for DNG/hydrogen (80/20) air mixture for ϕ = 1.4 and 1600 Re (T = 293K, p = 1 atm)

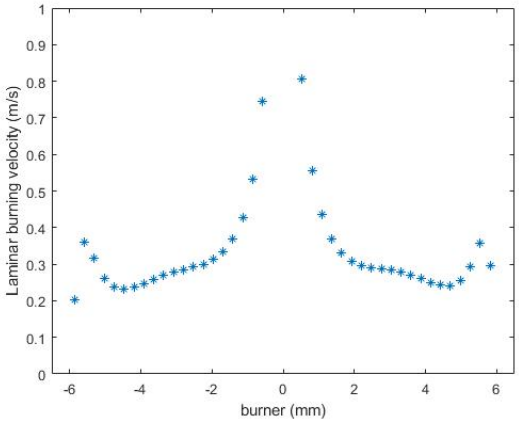

Figure 4.24: Laminar burning velocity versus flame front location for DNG/hydrogen (80/20) air mixture for ϕ = 1.4 and 1600 Re (T = 293K, p = 1 atm)

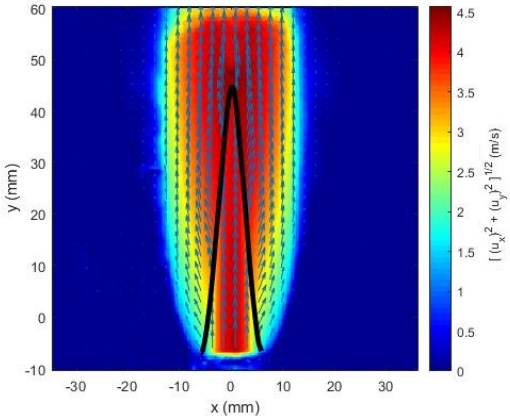

Figure 4.25: Velocity field for DNG/hydrogen (80/20) air mixture for ϕ = 1.4 and 1800 Re (T = 293K, p = 1 atm)

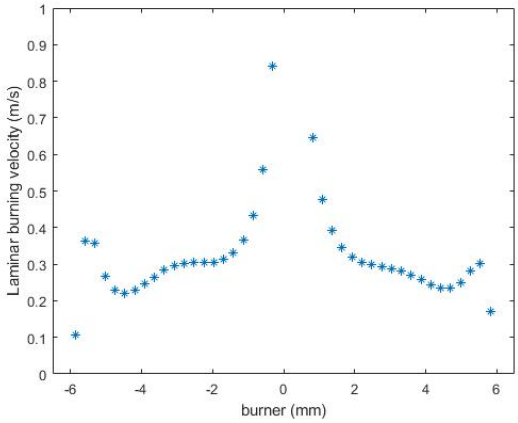

Figure 4.26: Laminar burning velocity versus flame front location for DNG/hydrogen (80/20) air mixture for ϕ = 1.4 and 1800 Re (T = 293K, p = 1 atm)

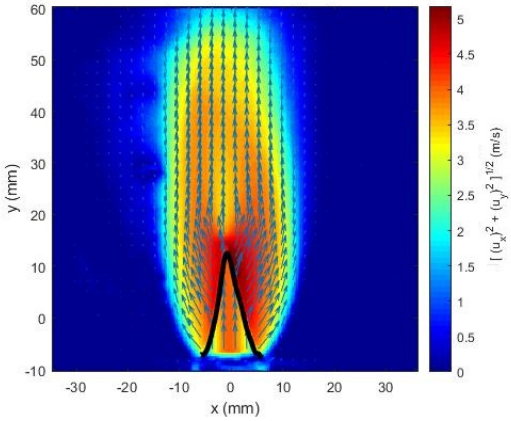

Figure 4.27: Velocity field for DNG/hydrogen (50/50) air mixture for ϕ = 1.0 and 1600 Re (T = 293K, p = 1 atm)

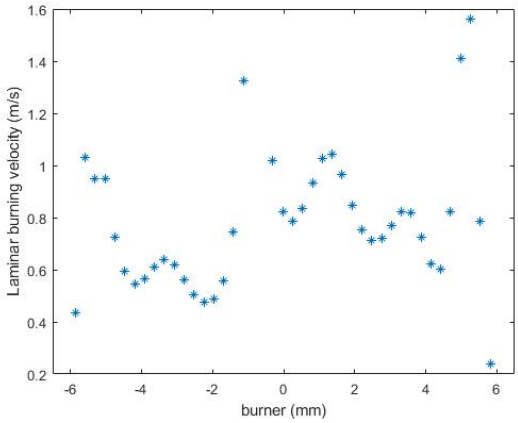

Figure 4.28: Laminar burning velocity versus flame front location for DNG/hydrogen (50/50) air mixture for ϕ = 1.0 and 1600 Re (T = 293K, p = 1 atm)

Table 4.13: Laminar burning velocities obtained from PIV at base of flame for DNG-hydrogen (80/20) air mixture at ϕ = 1.4 and 1600 and 1800 Re, compared with OH* and GRI-Mech 3.0 results (T = 293K, p = 1 atm)

Laminar burning velocity (cm/s)				**Difference wrt 1600 Re (%)**		
1600 Re	1800 Re	OH*	GRI-Mech 3.0	1800 Re	OH*	GRI-Mech 3.0
24.5	24.3	25.2	17.2	0.82	2.86	29.80

4.3.3. DNG-hydrogen (50/50) air mixture

DNG with 50% volumetric hydrogen addition air mixtures are measured for both equivalence ratio 1.0 and 1.4, at 1600 and 1800 Reynolds number. Figure4.27 shows the velocity field for equivalence ratio 1.0 and 1100 Re, with figure4.28 the corresponding laminar burning velocity plot over the flame front. Figure 4.29 shows the velocity field for equivalence ratio 1.4 and 1100 Re, with figure 4.30 the corresponding laminar burning velocity plot over the flame front. Figure 4.31 and 4.32 show the velocity field and laminar burning velocity over the flame front plot for equivalence ratio 1.4 and 1100 respectively. The velocity field and laminar burning velocity plot for Equivalence ratio 1.4 and 1600 Reynolds number are shown in figure 4.33 and 4.34 respectively.

Large fluctuations are observed for the 50% hydrogen addition measurements at 1.0 equivalence ratio, for both Reynolds numbers. This is most likely the case of significant disturbance on the velocity

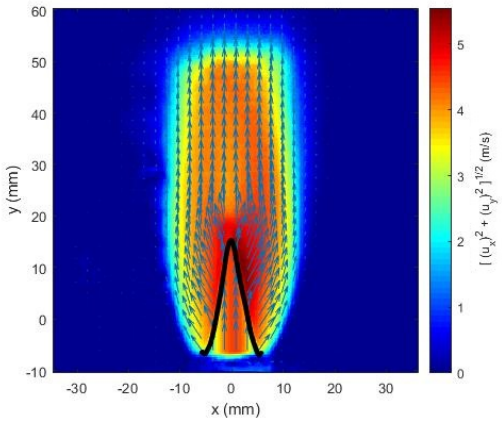

Figure 4.29: Velocity field for DNG/hydrogen (50/50) air mixture for ϕ = 1.0 and 1800 Re (T = 293K, p = 1 atm)

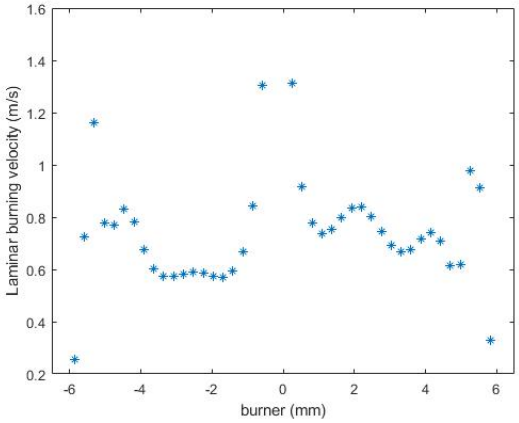

Figure 4.30: Laminar burning velocity versus flame front location for DNG/hydrogen (50/50) air mixture for ϕ = 1.0 and 1800 Re (T = 293K, p = 1 atm)

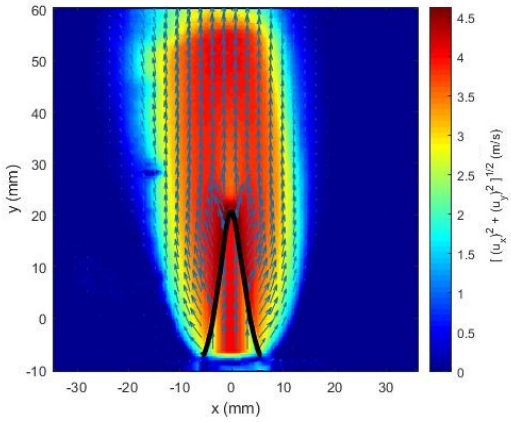

Figure 4.31: Velocity field for DNG/hydrogen (50/50) air mixture for ϕ = 1.4 and 1600 Re (T = 293K, p = 1 atm)

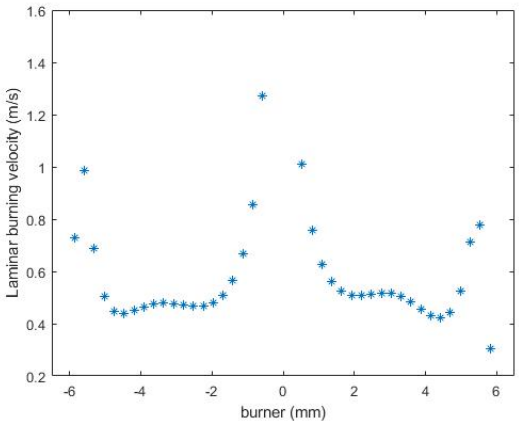

Figure 4.32: Laminar burning velocity versus flame front location for DNG/hydrogen (50/50) air mixture for ϕ = 1.4 and 1600 Re (T = 293K, p = 1 atm)

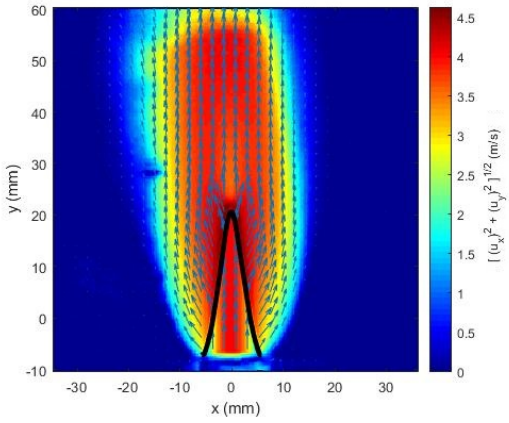

Figure 4.33: Velocity field for DNG/hydrogen (50/50) air mixture for ϕ = 1.4 and 1800 Re (T = 293K, p = 1 atm)

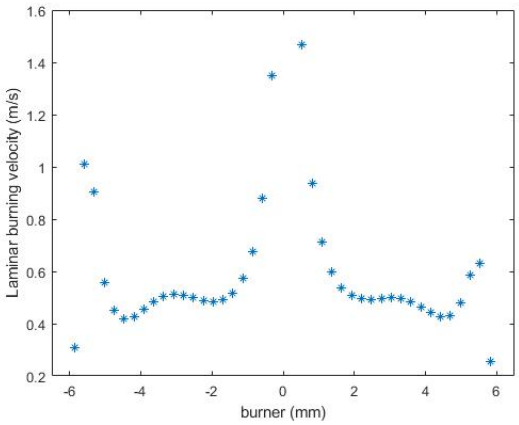

Figure 4.34: Laminar burning velocity versus flame front location for DNG/hydrogen (50/50) air mixture for ϕ = 1.4 and 1800 Re (T = 293K, p = 1 atm)

field due to the seeding particles. 50% hydrogen addition results in a significantly higher laminar burning velocity than the other cases, and thus the largest thermophoretic effects because of the large temperature gradient. The trend observed till now is that the higher the laminar burning velocity, the stronger the disturbance on the velocity field. 1.4 equivalence ratio measurements are significantly more stable. The instability of the flame cone can also be observed in figure 4.27 and 4.29 in the form of the tilting of the flame. This could be wrinkling of the flame due to the seeding disturbance being significant enough such that the flow becomes turbulent. The laminar burning velocity is still extracted from these measurements for consistency sake. The 50% measurements should however be approached with caution. Table 4.14 presents the laminar burning velocity obtained with PIV for 50% hydrogen addition mixtures for equivalence ratio 1.0 for both Reynolds numbers, and compared with OH* and GRI-Mech 3.0. As expected, the Reynolds numbers have a rather significant discrepancy of 16.8% between the two. The 1600 Reynolds number measurement is in good agreement with both OH* and GRI-Mech 3.0. Table 4.11 presents the PIV results for equivalence ratio 1.4 and Reynolds number 1100 and 1600. Both Reynolds numbers are also here in good agreement with each other and with the OH*-chemiluminescence measurement. However also in this case, as with the previous measurements, a large discrepancy of 22.22% is found compared to the GRI-Mech 3.0 for equivalence ratio 1.4. GRI-Mech 3.0 tends to underestimate the laminar burning velocity compared to the PIV and OH*-chemiluminescence results, also in the 50% hydrogen addition measurements.

Table 4.14: Laminar burning velocities obtained from PIV at base of flame for DNG-hydrogen (50/50) air mixture at ϕ = 1.0 and 1600 and 1800 Re, compared with OH* and GRI-Mech 3.0 results (T = 293K, p = 1 atm)

Laminar burning velocity (cm/s)				**Difference wrt 1600 Re (%)**		
1600 Re	1800 Re	OH*	GRI-Mech 3.0	1800 Re	OH*	GRI-Mech 3.0
59.4	69.4	57.0	57.9	16.8	4.04	2.53

Table 4.15: Laminar burning velocities obtained from PIV at base of flame for DNG-hydrogen (50/50) air mixture at ϕ = 1.4 and 1600 and 1800 Re, compared with OH* and GRI-Mech 3.0 results (T = 293K, p = 1 atm)

Laminar burning velocity (cm/s)				**Difference wrt 1600 Re (%)**		
1600 Re	1800 Re	OH*	GRI-Mech 3.0	1800 Re	OH*	GRI-Mech 3.0
44.1	43.5	45.1	34.3	1.36	2.23	22.22

4.4. Summarized results and discussion

Figure 4.35 shows the Laminar burning velocity comparison between experimental results of PIV and OH*, and simulated results using GRI-Mech 3.0 for DNG with 0, 20% and 50% hydrogen addition and air mixture at equivalence ratio 1.0. Error bars represent 95% confidence interval for the OH*-chemiluminescence measurements. The same measurements for equivalence ratio 1.4 are shown in figure 4.36.

The measurements from both independent measurement techniques, PIV and OH*, are in good agreement with each other for both equivalence ratios. The DNG/hydrogen measurements with OH*-chemiluminescence can be interpreted with great confidence due to the successful hydrogen validation methodology. Therefore conclusions can be drawn that PIV is a reliable method to obtain the laminar burning velocity without typical uncertainties found with OH*-chemiluminescence due to the mass flow controllers, since the actual velocity field is obtained. It was found, however, that the seeding disturbance and thermophoretic effects can have a significant effect on the PIV obtained laminar burning velocity. These influences should therefore be approached with care when using PIV. OH*-chemiluminescence shows a larger uncertainty interval due to the mass flow controllers. The advantages of this measurement technique however are the ease of use and low cost when compared to PIV.

The GRI-Mech 3.0 kinetic mechanism is an excellent agreement with both measurement techniques for equivalence ratio 1.0 but has a significant deviation for equivalence ratio 1.4. Possible explanations for this discrepancy is the changing natural gas composition over time, or the inability for the numerical solver to capture the rich region of this particular fuel composition.

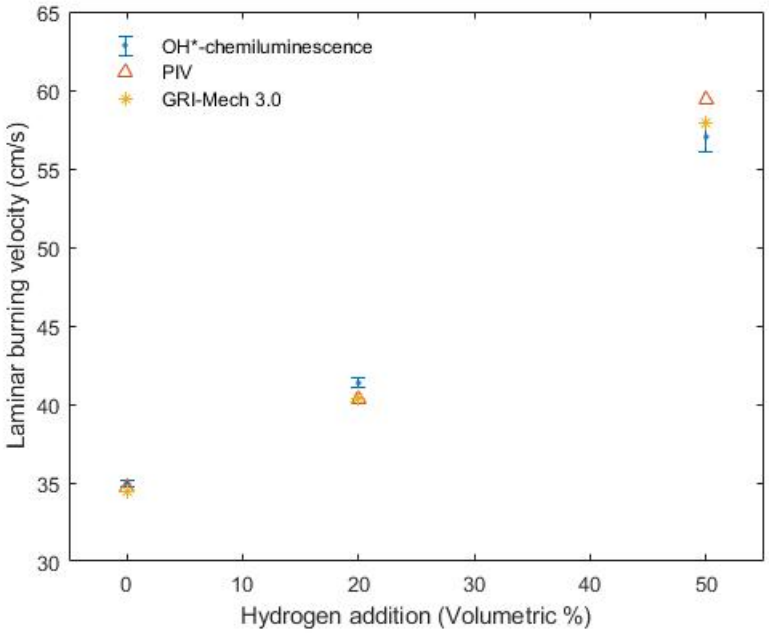

Figure 4.35: Laminar burning velocity comparison between experimental results of PIV and OH*, and simulated results using GRI-Mech 3.0 for DNG with 0, 20% and 50% hydrogen addition and air mixture at equivalence ratio 1.0. Error bars represent 95% confidence interval for the OH*-chemiluminescence measurements (T = 293 K, p = 1 atm)

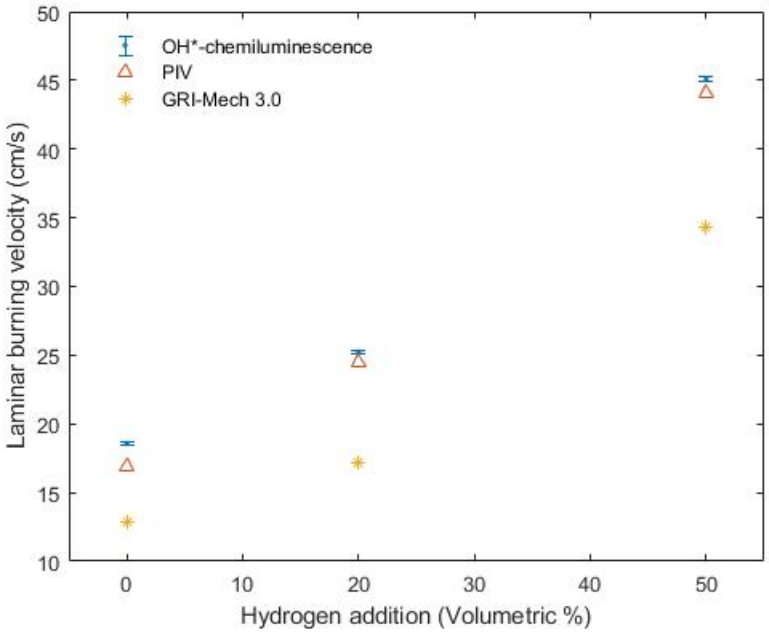

Figure 4.36: Laminar burning velocity comparison between experimental results of PIV and OH*, and simulated results using GRI-Mech 3.0 for DNG with 0, 20% and 50% hydrogen addition and air mixture at equivalence ratio 1.4. Error bars represent 95% confidence interval for the OH*-chemiluminescence measurements (T = 293 K, p = 1 atm)

5

Conclusion and recommendations

5.1. Conclusions

The laminar burning velocity is an important property of combustion mixtures. It contains fundamental information on reactivity, exothermicity and diffusivity. This thesis has investigated the laminar burning velocity of Dutch natural gas - hydrogen mixtures numerically and experimentally. The volumetric addition of hydrogen up to 50% was investigated in increments of 10% . Experimental measurements were performed with the Bunsen burner method. Two methodologies were applied to obtain the laminar burning velocity. The mass conservation method was used in combination with the OH*-chemiluminescence. The second methodology used the semi-cone angle method in combination with particle image velocimetry (PIV). 12 different conditions were measured with PIV. These points are for 3 different fuel compositions (0, 20 and 50% H_2), two different equivalence ratios (1.0 and 1.4) and two different flow conditions (1100/1600 and 1800 Reynolds). The PIV methodology was compared with both OH*-chemiluminescence and the numerical calculations. The effect on the flow conditions was also investigated on the laminar burning velocity obtained. Numerical predictions were obtained with the GRI-Mech 3.0 kinetic mechanism. Preliminary measurements were performed with 100% hydrogen in order to validate the optical diagnostics and post-processing procedure for the OH*-chemiluminescence methodology. The following conclusions can be drawn from this thesis:

- The 100% hydrogen predictions with GRI-Mech 3.0 kinetic mechanism predictions are overestimating the laminar burning velocities compared to the experimental results. This trend is mainly because the experimental results are not adiabatic due to the heat losses and the stretch effects. The numerical results are for adiabatic unstretched flames. A discrepancy between the laminar burning velocity obtained from OH*-chemiluminescence and GRI-Mech 3.0 numerical predictions for equivalence ratio 1 is 17.8% . The difference tends to decrease with increasing equivalence ratio, and is around 6% for the rich region. Experimental hydrogen measurements, when compared to experimental results in the literature, show that the overall agreement between the different studies is generally good.
- The OH*-chemiluminescence measurements are presented with a 95% confidence interval. The maximum laminar burning velocity increases from 35.3 $\pm$ 0.2 cm/s (0% H_2) to 37.2 $\pm$ 0.3 cm/s (10% H_2), 41.4 $\pm$ 0.2 cm/s (20% H_2), 46.3 $\pm$ 0.3 cm/s (30% H_2), 52.9 $\pm$ 0.3 cm/s (40% H_2) and 62.2 $\pm$ 0.4 cm/s (50% H_2). All maximum burning velocities are achieved for equivalence ratio 1.1.
- Different flow conditions have minimal effect on the obtained laminar burning velocity. The discrepancy between the two flow conditions are in the range 0.82% - 7.69%. Only one measurement protrudes above all with a 16.8% discrepancy, due to the disturbance of the seeding particles on the flow. The seeding density should therefore be approached with care as it has a significant effect on the obtained laminar burning velocity.
- The measurements from both independent measurement techniques, PIV and OH*, are in good agreement with each other for both equivalence ratio 1.0 and 1.4. The discrepancies are in the

range 0.86% - 4.04% with one outliner of 10.1%. The DNG/hydrogen measurements with OH*-chemiluminescence can be interpreted with great confidence due to the successful hydrogen validation methodology. Therefore conclusions can be drawn that PIV is a reliable method to obtain the laminar burning velocity without typical uncertainties found with OH*-chemiluminescence due to the mass flow controllers, since the actual velocity field is obtained. OH*-chemiluminescence shows a larger uncertainty interval due to the mass flow controllers. The advantages of this measurement technique however are the ease of use and low cost when compared to PIV.

- Numerical results from GRI-Mech 3.0 are in good agreement with OH*-chemiluminescence and PIV results for equivalence ratio <1.2. Large discrepancies, between 20-35%, are observed in the rich region for equivalence ratio 1.3 - 1.5 This discrepancy is consistent with both PIV and OH*-chemiluminescence measurements. This discrepancy could be attributed to the validity of the kinetic mechanism for the composition of DNG, which contains methane with higher order hydrocarbons and 14% N_2, in the rich region. The DNG from the Dutch gas network could also have a different composition than the one used for the numerical simulation resulting in different laminar burning velocities.

5.2. Recommendations

- Fuel compositions for 0-30% H_2 addition experienced blow-off before reaching the proposed equivalence ratio measurement range of 0.8. This is the result of the entrainment of outside air at the burner rim, resulting in dilution of the fuel mixture. By using a coflow burner with an inert gas, for example N_2, the Bunsen flame can be isolated from entrainment effects of the outside air.
- In this work, the optical diagnostics and post-processing for the OH*-chemiluminescence were validated with hydrogen measurements. This however does not fully validate the methodology, since the hydrogen measurements use a different burner diameter. In order to also validate the burner for the DNG hydrogen measurements, 100% methane or another hydrocarbon has to be measured and compared with existing literature. The could not be performed for this thesis because methane was not available in the laboratory.
- The seeders used for the PIV measurements were not designed for the proposed mass flows. This resulted in an uneven flow of seeding and resulted in a significant disturbance in the velocity field for certain measurements. The recommendation is therefore to carefully select the seeding devices such that a non-intrusive constant flow of seeding is mixed with the unburned gases.
- The characteristics for higher volumetric hydrogen additions to DNG should be investigated. Addition of hydrogen results in an exponential increase of the laminar burning velocity. Therefore the burner design parameters have to be reevaluated when increasing the hydrogen addition even further.
- Operating near the lower limits of the mass flow controllers results in more fluctuations in the mass flows. The full scale of the mass flow controllers for all three gases (hydrogen, DNG and air) were also significantly larger than the mass flow ranges used in the experiments. More accurate mass flow controllers which better suit the operational range of the measurements should therefore be used.
- One possible argument for the discrepancy between the experimental and numerical results in the rich region was attributed to the change of fuel composition. To further investigate this point, DNG measurements have to be taken for the full equivalence ratio range, on different days. These measurements could then be compared and a discrepancy could suggest a change in the natural gas composition.
- In the literature several combustion reaction mechanisms can be found, which are often developed and validated for specific situations and fuel compositions. The GRI-Mech 3.0 was selected in this thesis as it is a prominent kinetic mechanism for natural gas combustion. Further investigation should be done on the numerical DNG hydrogen laminar burning velocities for different

kinetic mechanisms. A comparison should be made between the numerical results and the experimental OH*-chemiluminescence and PIV measurements. Important kinetic mechanisms which contain the species present in DNG hydrogen mixtures are for example Konnov [84] and GDF-Kin 3.0 mechanism [85].

Bibliography

[1] I. Glassman, R. A. Yetter, and N. G. Glumac, *Combustion* (Academic press, 2014).

[2] C. Law, *Dynamics of stretched flames,* in *Symposium (International) on Combustion*, Vol. 22 (Elsevier, 1989) pp. 1381–1402.

[3] N. Lamoureux, N. Djebaıli-Chaumeix, and C.-E. Paillard, *Laminar flame velocity determination for h2–air–he–co2 mixtures using the spherical bomb method,* Experimental Thermal and Fluid Science **27**, 385 (2003).

[4] C. J. Rallis and A. M. Garforth, *The determination of laminar burning velocity,* Progress in Energy and Combustion Science **6**, 303 (1980).

[5] P. Stamatoglou, *Spectral analysis of flame emission for optimization of combustion devices on marine vessels,* Lund Reports on Combustion Physics LRCP-176 (2014).

[6] N. Bouvet, C. Chauveau, I. Gökalp, S. Y. Lee, and R. J. Santoro, *Characterization of syngas laminar flames using the Bunsen burner configuration,* International Journal of Hydrogen Energy **36**, 992 (2011).

[7] H. Ishida, *Lift-off and blow-off of laminar jet premixed flame of flammable mixture with inert gas,* RESEARCH REPORTS , 25 (2004).

[8] Y. Wu, V. Modica, B. Rossow, and F. Grisch, *Effects of pressure and preheating temperature on the laminar flame speed of methane/air and acetone/air mixtures,* Fuel **185**, 577 (2016).

[9] E. Polman, J. De Laat, M. Crowther, *et al.*, *Reduction of co2 emissions by adding hydrogen to natural gas,* IEA Green House Gas R&D programme (2003).

[10] J. Gigler and M. Weeda, *Outlines of a hydrogen roadmap,* TKI NIEUW GAS Topsector Energie (2018).

[11] L. Ben, G. Charnay, and R. Truquet, *Influence of air/ fuel ratio on cyclic variation and exhaust emission in natural gas si engine. sae paper 992901, 1999,* .

[12] S. Rousseau, B. Lemoult, and M. Tazerout, *Combustion characterization of natural gas in a lean burn spark-ignition engine,* Proceedings of the Institution of Mechanical Engineers, Part D: Journal of Automobile Engineering **213**, 481 (1999).

[13] A. Das and H. Watson, *Development of a natural gas spark ignition engine for optimum performance,* Proceedings of the Institution of Mechanical Engineers, Part D: Journal of Automobile Engineering **211**, 361 (1997).

[14] K. Hughes, T. Turanyi, A. Clague, and M. Pilling, *Development and testing of a comprehensive chemical mechanism for the oxidation of methane,* International Journal of Chemical Kinetics **33**, 513 (2001).

[15] C. K. Law, *Combustion physics* (Cambridge university press, 2010).

[16] A. H. Lefebvre, *Gas turbine combustion: alternative fuels and emissions* (CRC press, 2010).

[17] R. J. Tabaczynski, F. H. Trinker, and B. A. Shannon, *Further refinement and validation of a turbulent flame propagation model for spark-ignition engines,* Combustion and Flame **39**, 111 (1980).

[18] G. L. Dugger, D. M. Simon, and M. Gerstein, *Laminar flame propagation,* NACA Report **1300**, 127 (1959).

[19] R. M. Fristrom and A. A. Westenberg, *Flame structure* (McGraw-Hill, 1965).

[20] A. A. Konnov, R. Meuwissen, and L. De Goey, *The temperature dependence of the laminar burning velocity of ethanol flames,* Proceedings of the Combustion Institute **33**, 1011 (2011).

[21] A. A. Konnov, *The temperature and pressure dependences of the laminar burning velocity: experiments and modelling,* in *Proceedings of the European Combustion Meeting–2015. Budapest, Hungary* (2015).

[22] F. Williams, *Analytical and numerical methods for investigation of flow fields with chemical reactions, especially related to combustion,* in *AGARD Conference Proceedings No*, Vol. 164 (1975).

[23] J. Buckmaster, *Two examples of a stretched flame,* The Quarterly Journal of Mechanics and Applied Mathematics **35**, 249 (1982).

[24] M. Matalon, *On flame stretch,* Combustion Science and Technology **31**, 169 (1983).

[25] S. Chung and C. Law, *An invariant derivation of flame stretch,* (1984).

[26] H. Kobayashi, Y. Kawabata, and K. Maruta, *Experimental study on general correlation of turbulent burning velocity at high pressure,* in *Symposium (International) on Combustion*, Vol. 27 (Elsevier, 1998) pp. 941–948.

[27] A. Lipatnikov and J. Chomiak, *Turbulent flame speed and thickness: phenomenology, evaluation, and application in multi-dimensional simulations,* Progress in energy and combustion science **28**, 1 (2002).

[28] R. Günther and G. Janisch, *Measurements of burning velocity in a flat flame front,* Combustion and Flame **19**, 49 (1972).

[29] F. Egolfopoulos, P. Cho, and C. Law, *Laminar flame speeds of methane-air mixtures under reduced and elevated pressures,* Combustion and flame **76**, 375 (1989).

[30] J. Natarajan, T. Lieuwen, and J. Seitzman, *Laminar flame speeds of H2/CO mixtures: Effect of CO2 dilution, preheat temperature, and pressure,* Combustion and Flame **151**, 104 (2007).

[31] M. Hassan, K. Aung, and G. Faeth, *Measured and predicted properties of laminar premixed methane/air flames at various pressures,* Combustion and Flame **115**, 539 (1998).

[32] T. Tahtouh, F. Halter, and C. Mounaïm-Rousselle, *Measurement of laminar burning speeds and markstein lengths using a novel methodology,* Combustion and Flame **156**, 1735 (2009).

[33] C. M. Vagelopoulos and F. N. Egolfopoulos, *Direct experimental determination of laminar flame speeds,* in *Symposium (international) on combustion*, Vol. 27 (Elsevier, 1998) pp. 513–519.

[34] Y. Dong, C. M. Vagelopoulos, G. R. Spedding, and F. N. Egolfopoulos, *Measurement of laminar flame speeds through digital particle image velocimetry: mixtures of methane and ethane with hydrogen, oxygen, nitrogen, and helium,* Proceedings of the combustion institute **29**, 1419 (2002).

[35] A. Van Maaren, D. Thung, and L. R. H. DE GOEY, *Measurement of flame temperature and adiabatic burning velocity of methane/air mixtures,* Combustion Science and Technology **96**, 327 (1994).

[36] I. Dyakov, A. A. Konnov, J. D. Ruyck, K. Bosschaart, E. Brock, and L. De Goey, *Measurement of adiabatic burning velocity in methane-oxygen-nitrogen mixtures,* Combustion Science and Technology **172**, 81 (2001).

[37] V. R. Kishore, N. Duhan, M. Ravi, and A. Ray, *Measurement of adiabatic burning velocity in natural gas-like mixtures,* Experimental Thermal and Fluid Science **33**, 10 (2008).

[38] M. Metghalchi and J. C. Keck, *Laminar burning velocity of propane-air mixtures at high temperature and pressure,* Combustion and flame **38**, 143 (1980).

[39] F. Egolfopoulos, D. Zhu, and C. Law, *Experimental and numerical determination of laminar flame speeds: mixtures of c2-hydrocarbons with oxygen and nitrogen,* in *Symposium (International) on Combustion*, Vol. 23 (Elsevier, 1991) pp. 471–478.

[40] C. Vagelopoulos, F. Egolfopoulos, and C. Law, *Further considerations on the determination of laminar flame speeds with the counterflow twin-flame technique,* in *Symposium (international) on combustion*, Vol. 25 (Elsevier, 1994) pp. 1341–1347.

[41] G. Jomaas, X. Zheng, D. Zhu, and C. Law, *Experimental determination of counterflow ignition temperatures and laminar flame speeds of c2–c3 hydrocarbons at atmospheric and elevated pressures,* Proceedings of the Combustion Institute **30**, 193 (2005).

[42] A. A. Konnov, I. V. Dyakov, and J. De Ruyck, *Measurement of adiabatic burning velocity in ethane–oxygen–nitrogen and in ethane–oxygen–argon mixtures,* Experimental thermal and fluid science **27**, 379 (2003).

[43] A. Huzayyin, H. Moneib, M. Shehatta, and A. Attia, *Laminar burning velocity and explosion index of lpg–air and propane–air mixtures,* Fuel **87**, 39 (2008).

[44] K. Bosschaart and L. De Goey, *The laminar burning velocity of flames propagating in mixtures of hydrocarbons and air measured with the heat flux method,* Combustion and Flame **136**, 261 (2004).

[45] S. Davis and C. Law, *Determination of and fuel structure effects on laminar flame speeds of c1 to c8 hydrocarbons,* Combustion Science and Technology **140**, 427 (1998).

[46] T. Hirasawa, C. Sung, A. Joshi, Z. Yang, H. Wang, and C. Law, *Determination of laminar flame speeds using digital particle image velocimetry: binary fuel blends of ethylene, n-butane, and toluene,* Proceedings of the Combustion Institute **29**, 1427 (2002).

[47] P. Dirrenberger, H. Le Gall, R. Bounaceur, O. Herbinet, P.-A. Glaude, A. Konnov, and F. Battin-Leclerc, *Measurements of laminar flame velocity for components of natural gas,* Energy & fuels **25**, 3875 (2011).

[48] Z. Huang, Y. Zhang, K. Zeng, B. Liu, Q. Wang, and D. Jiang, *Measurements of laminar burning velocities for natural gas–hydrogen–air mixtures,* Combustion and Flame **146**, 302 (2006).

[49] G. Yu, C. Law, and C. Wu, *Laminar flame speeds of hydrocarbon+ air mixtures with hydrogen addition,* Combustion and Flame **63**, 339 (1986).

[50] F. Halter, C. Chauveau, N. Djebaili-Chaumeix, and I. Gökalp, *Characterization of the effects of pressure and hydrogen concentration on laminar burning velocities of methane–hydrogen–air mixtures,* Proceedings of the Combustion Institute **30**, 201 (2005).

[51] E. Hu, Z. Huang, J. He, C. Jin, and J. Zheng, *Experimental and numerical study on laminar burning characteristics of premixed methane–hydrogen–air flames,* international journal of hydrogen energy **34**, 4876 (2009).

[52] F. Coppens, J. De Ruyck, and A. A. Konnov, *The effects of composition on burning velocity and nitric oxide formation in laminar premixed flames of ch4+ h2+ o2+ n2,* Combustion and Flame **149**, 409 (2007).

[53] R. Hermanns, A. A. Konnov, R. Bastiaans, L. De Goey, K. Lucka, and H. Köhne, *Effects of temperature and composition on the laminar burning velocity of ch4+ h2+ o2+ n2 flames,* Fuel **89**, 114 (2010).

[54] C. W. Choi and I. K. Puri, *Contribution of curvature to flame-stretch effects on premixed flames,* Combustion and flame **126**, 1640 (2001).

[55] D. Kurtuluş, C. Cohé, C. Chauveau, and I. Gökalp, *Characterisation of lean premixed laminar flames in high pressure using piv,* .

[56] D. G. Goodwin, H. K. Moffat, and R. L. Speth, *Cantera: An object-oriented software toolkit for chemical kinetics, thermodynamics, and transport processes,* http://www.cantera.org (2017), version 2.3.0.

[57] N. Docquier, S. Belhalfaoui, F. Lacas, N. Darabiha, and C. Rolon, *Experimental and numerical study of chemiluminescence in methane/air high-pressure flames for active control applications,* Proceedings of the combustion institute **28**, 1765 (2000).

[58] T. Zhang, Q. Guo, Q. Liang, Z. Dai, and G. Yu, *Distribution characteristics of oh*, ch*, and c2* luminescence in ch4/o2 co-flow diffusion flames,* Energy & Fuels **26**, 5503 (2012).

[59] M. F. N. W. M. B. E. M. G. C. T. B. R. K. H. S. S. W. C. G. J. V. V. L. Gregory P. Smith, David M. Golden and Z. Qin, *Gri-mech 3.0,* http://combustion.berkeley.edu/gri-mech/version30/text30.html#cite (2017).

[60] K. Avila, D. Moxey, A. de Lozar, M. Avila, D. Barkley, and B. Hof, *The onset of turbulence in pipe flow,* Science **333**, 192 (2011).

[61] *Bornkhorst mass flow meters and controllers, howpublished = https://www.bronkhorst.com/, note = Accessed: 18-07-2018,* .

[62] G. M. Clarke and D. Cooke, *A basic course in statistics*, Tech. Rep. (Edward Arnold London, 1978).

[63] R. D. Keane and R. J. Adrian, *Theory of cross-correlation analysis of piv images,* Applied scientific research **49**, 191 (1992).

[64] DaVis 10, *Software solution for intelligent imaging,* (<2017>).

[65] Pivmat, *Matlab toolbox,* (<2017>).

[66] F. Scholz, *Tolerance stack analysis methods,* Research and technology boeing information & support services, boeing, seattle , 1 (1995).

[67] A. Konnov, *The effect of temperature on the adiabatic laminar burning velocities of ch4- air and h2- air flames,* Fuel **89**, 2211 (2010).

[68] G. Andrews and D. Bradley, *Determination of burning velocities: a critical review,* Combustion and Flame **18**, 133 (1972).

[69] C. T. Chong and S. Hochgreb, *Measurements of laminar flame speeds of acetone/methane/air mixtures,* Combustion and Flame **158**, 490 (2011).

[70] C. Sung, J. Kistler, M. Nishioka, and C. Law, *Further studies on effects of thermophoresis on seeding particles in ldv measurements of strained flames,* Combustion and flame **105**, 189 (1996).

[71] C. Tropea and A. L. Yarin, *Springer handbook of experimental fluid mechanics*, Vol. 1 (Springer Science & Business Media, 2007).

[72] D. R. Dowdy, D. B. Smith, S. C. Taylor, and A. Williams, *The use of expanding spherical flames to determine burning velocities and stretch effects in hydrogen/air mixtures,* in *Symposium (International) on Combustion*, Vol. 23 (Elsevier, 1991) pp. 325–332.

[73] K. Aung, M. Hassan, and G. Faeth, *Flame stretch interactions of laminar premixed hydrogen/air flames at normal temperature and pressure,* Combustion and flame **109**, 1 (1997).

[74] S. Tse, D. Zhu, and C. Law, *Morphology and burning rates of expanding spherical flames in h2/o2/inert mixtures up to 60 atmospheres,* Proceedings of the Combustion Institute **28**, 1793 (2000).

[75] T. Iijima and T. Takeno, *Effects of temperature and pressure on burning velocity,* Combustion and flame **65**, 35 (1986).

[76] N. Lamoureux, N. Djebaili-Chaumeix, and C. Paillard, *Laminar flame velocity determination for h _2-air-steam mixtures using the spherical bomb method,* in *Journal de Physique IV (Proceedings)*, Vol. 12 (EDP sciences, 2002) pp. 445–452.

[77] C. Dong, Q. Zhou, Q. Zhao, Y. Zhang, T. Xu, and S. Hui, *Experimental study on the laminar flame speed of hydrogen/carbon monoxide/air mixtures,* Fuel **88**, 1858 (2009).

[78] C. Wu and C. K. Law, *On the determination of laminar flame speeds from stretched flames,* in *Symposium (International) on Combustion*, Vol. 20 (Elsevier, 1985) pp. 1941–1949.

[79] M. Mizomoto and H. Yoshida, *Effects of lewis number on the burning intensity of bunsen flames,* Combustion and flame **70**, 47 (1987).

[80] J. Wang, Z. Wei, S. Yu, W. Jin, Y. Xie, M. Zhang, and Z. Huang, *Effects of stretch and preferential diffusion on tip opening of laminar premixed bunsen flames of syngas/air mixtures,* Fuel **148**, 1 (2015).

[81] G. Kozlovsky and G. Sivashinsky, *On open and closed tips of bunsen burner flames,* Theoretical and Computational Fluid Dynamics **6**, 181 (1994).

[82] *Rijkstdienst van ondernemend nederland, howpublished = https://www.rvo.nl/onderwerpen/duurzaam-ondernemen/energie-en-milieu-innovaties/gassamenstelling, note = Accessed: 13-11-2018,* .

[83] D. Bradley, S. E.-D. Habik, and S. El-Sherif, *A generalization of laminar burning velocities and volumetric heat release rates,* Combustion and flame **87**, 336 (1991).

[84] A. A. Konnov, *Remaining uncertainties in the kinetic mechanism of hydrogen combustion,* Combustion and flame **152**, 507 (2008).

[85] L. Pillier, P. Desgroux, B. Lefort, L. Gasnot, J. Pauwels, I. Da Costa, *et al.*, *No prediction in natural gas flames using gdf-kin® 3.0 mechanism ncn and hcn contribution to prompt-no formation,* Fuel **85**, 896 (2006).